Astron. Astrophys. 323, 566–584 (1997)

ASTRONOMY
AND
ASTROPHYSICS

A unified model of interstellar dust

Aigen Li and J. Mayo Greenberg

Laboratory Astrophysics, University of Leiden, Postbus 9504, 2300 RA Leiden, The Netherlands
(agli@strw.LeidenUniv.nl; mayo@rulhl1.LeidenUniv.nl)

Received 12 October 1996 / Accepted 10 January 1997

Abstract. We have simultaneously modeled both the interstellar extinction and polarization (both linear and circular) on the basis of a trimodal dust model: large silicate core-organic refractory mantle dust particles; very small carbonaceous particles responsible for the hump extinction; and PAH's responsible for the FUV extinction. The core-mantle particles which are the exclusive contributor to the interstellar polarization and the dominant contributor to the visual and NIR extinction are modeled as finite cylinders with a Gaussian size distribution in terms of perfect spinning alignment. Results for models using infinite cylinders are presented for comparison. Our model results are in good agreement with such observational constraints as the average interstellar extinction curve, the polarization law, the ratio of visual polarization to extinction $(P/A)_v$, the scattering properties (albedos), the excess NIR polarization over the extrapolation of the Serkowski law. The $(P/A)_v$ constraint imposed on other dust models (e.g., the silicate/graphite model, the composite dust model) leads to either a too low $(P/A)_v$ value (the silicate/graphite model) or instability of particle structure (the composite dust model). The cosmic abundance constraints, in particular the evidence for lower oxygen abundance in the interstellar medium than in the solar system and the possible interstellar C/O ratios, are discussed extensively. Considering the uncertainties in the interstellar "cosmic" abundances, the C/O ratio and the interstellar non-dust elemental abundances, although our model requires a bit more carbon than the reference abundance, it is within the limit of an acceptable range and is a significant improvement over other models. All the other major reference abundance (cosmic - non-dust) constraints on O, N, Si, Mg, Fe are well satisfied.

Key words: ISM: dust, extinction – polarization – scattering – ISM: abundances – ultraviolet: ISM – infrared: ISM: continuum

1. Introduction

The physical and chemical nature of interstellar dust grains such as composition, size, shape, alignment etc. are largely determined from the observations of interstellar continuum extinction, polarization and dust thermal emission (for a recent review see Dorschner & Henning 1996). The constraints on any dust model are both direct and indirect. The direct ones are optical: 1) wavelength (λ) dependence of extinction; 2) wavelength dependence of polarization; 3) ratio of polarization-to-extinction; 4) absorption and emission spectra. The indirect ones are astrophysical: 5) cosmic abundances of the condensable elements; 6) material survivability — sources and sinks. Any dust model, to be considered successful, should satisfy all six constraints. It is the aim of the present paper to produce a model which in all respects exhibits no inconsistencies with these conditions. A unified model ... This should not be taken as a pretentious title. It mainly reflects the idea that the same particles are responsible for *both* the extinction and polarization. These represent the major fraction of the total dust mass — about 80% (Greenberg & Li 1995; Block et al. 1994). It has always seemed reasonable to one of us (JMG) to expect this to be the case since it became known that variations in extinction and polarization have a certain degree of correlation in the sense that when the extinction appeared to be due to, say, large or smaller particles, so too did the polarization. We have come a long way since the second paper with the same title was published (Hong & Greenberg 1980) and a really great deal has been learned about dust and the interstellar medium since the first paper (Greenberg & Shah 1967). Spectral information in the infrared has also provided many strong constraints on the dust populations.

Recently successful attempts have been made to obtain both interstellar extinction and polarization observational data in the far ultraviolet (hereafter FUV) and the near infrared (hereafter NIR) where the data were earlier unavailable. Observations have also been carried out for more lines of sight, including not only the diffuse cloud medium, but also in dark molecular clouds and star forming regions. The observations have confirmed that there is a "generally" quite uniform type of interstellar extinction law — the wavelength dependent extinction curve rises from the NIR to the near ultraviolet, generally with a prominent hump centered at $\sim 4.6\,\mu\mathrm{m}^{-1}$, followed by a steep rise into the FUV (see, e.g., Greenberg & Chlewicki 1983; Savage & Mathis 1979; etc.). It has been shown by Cardelli et al. (1989) (hereafter CCM) that, the extinction law can largely be characterized

Send offprint requests to: J.M. Greenberg

by a single parameter, the ratio of total to selective extinction, $R_v = A_v/E(B-V)$. This actually reflects the evolutionary state of dust grains in different astrophysical environments as indicated by the cyclic dust model (Greenberg 1982; Greenberg 1986).

The wavelength dependent polarization in the visual/near ultraviolet may be represented by the so-called Serkowski empirical law

$$P(\lambda)/P_{max} = exp\,[-K\,ln^2(\lambda/\lambda_{max})], \quad (1)$$

where P_{max} is the maximum polarization and λ_{max} is the wavelength where P_{max} occurs (Serkowski 1973; Coyne et al. 1974; Wilking et al. 1982). The width parameter K which was originally taken as constant (Serkowski 1973; Coyne et al. 1974) was shown to vary systematically with λ_{max}, $K \approx 1.66\,\lambda_{max} + 0.01$ (Whittet et al. 1992 and references therein). The near infrared polarization has been found to be higher than that extrapolated from the Serkowski law (Martin et al. 1992). It was suggested by Martin et al. (1992) and Martin & Whittet (1990) that a common power law $P(\lambda) \propto \lambda^{-\beta}$ might be more representative of the interstellar near infrared polarization (than the Serkowski law) where the power index β is independent of λ_{max} and in the range of 1.6 to 2.0, $\beta \simeq 1.8 \pm 0.2$. The FUV polarization observations only became available in recent years as a consequence of the Wisconsin Ultraviolet Photo-Polarimetry Experiment (WUPPE) (Clayton et al. 1992) and the ultraviolet polarimetry of the Hubble Space Telescope (Somerville et al. 1994; Clayton et al. 1995). These observations indicate that the FUV polarization might be divided into 3 categories: (1) Serkowski law — those with $\lambda_{max} \geq 0.54\mu$m which are consistent with the extrapolated Serkowski law; (2) Super-Serkowski law — those with $\lambda_{max} \leq 0.53\mu$m which show polarization in excess of the extrapolated Serkowski law; (3) Hump polarization — those with a polarization feature which seems to be associated with the 4.6 μm^{-1} extinction hump (Clayton et al. 1992; Anderson et al. 1996). If both the hump excess polarization and the hump extinction are really produced by the same carrier (the hump particles), the degree of alignment and/or polarizability of such particles should be very small. For example, along the line of sight to HD 197770, the ratio of the excess polarization to the hump extinction is $P_H/A_H \simeq 0.002$ while the polarization to extinction ratio in the visual is $P_v/A_v \simeq 0.025$, thus $\frac{P_H}{A_H}/\frac{P_v}{A_v}$ is only ~ 0.09, so that, the contribution of the hump particles to the polarization in the visual would be much smaller than that by the core-mantle particles. In fact, we shall find in our model that $A_H(v)/A_v \leq 0.05$ so that $P_H(v)/P_v \simeq 0.005$. Therefore we will not take the hump polarization into account in our model.

With the availability of the additional recent NIR and FUV observational data along with the visible data, it is possible to place more constraints on interstellar dust models than before. Recent progress in cosmic abundance research (e.g.; Snow & Witt 1996; Cardelli et al. 1996) has consistently indicated that the condensable elements (O, C, N, Mg, Fe, Si) are less abundant in the general interstellar medium than in the solar system. Whereas, on the one hand, the solar system abundances were considered to be too high to be accounted for by the observed dust and gas (Greenberg 1974), the currently accepted abundances put rather strong limits on the dust models. In this work, we are trying to model simultaneously both the interstellar extinction and polarization from the NIR to FUV. For simplicity we only consider the average diffuse cloud medium case, namely $R_v = 3.1$ and $\lambda_{max} \sim 0.55\mu$m. We fully recognize that an average actually may represent a variety of individual cases and, in the future, we shall consider how these can be fitted with parameter variations consistent with the basic astrophysical constraints. We believe that a reliable fit to the average provides the key to understanding the variations.

The grain shape is far from well established, partly due to the lack of exact solutions of the scattering properties of particles of arbitrary shape (van de Hulst 1957). Actually, rigorous solutions only exist for spheres (Mie 1908) and infinite cylinders (Lind & Greenberg 1966; Shah 1970). The assumption of spheres should be precluded, (except for some illustrative examples), because of the interstellar polarization; and while infinite cylinders are suitable for qualitative examples of interstellar polarization they produce unreal scattering in the long wavelength limit, i.e., $Q_{sca} \propto \lambda^{-3}$, instead of $Q_{sca} \propto \lambda^{-4}$ which applies for finite size particles (Martin 1978). This excessive scattering by two dimensional particles was noted in van de Bult, Greenberg & Whittet (1985) where the scattering cross section in the infrared was ignored in calculating the ice band extinction shapes in the infrared for infinite cylinders.

Although many methods have been developed to investigate more realistic shapes; e.g., the Fourier analysis solution of the boundary-value problem for spheroids (Asano & Yamamoto 1975); the Fredholm integral equation method (Holt et al. 1978) for ellipsoidal particles; the volume integral equation formulation (VIEF) in which the Maxwell equations are solved in integral form (Hage & Greenberg 1990) for particles with arbitrary shapes; the DDA (discrete dipole approximation) method (Purcell & Pennypacker 1973; Draine 1988) for arbitrarily-shaped particles in which the particles are replaced by an array of electric dipoles; the separation of variables method (Voshchinnikov & Farafonov 1993) for spheroids; the T-matrix method in principle useful for particles of arbitrary shape but practically mostly for axisymmetric particles (Waterman & McCarthy 1968; Barber & Yeh 1975; Barber & Hill 1990); and recently, Rouleau (1996) developed a method to investigate the optical properties of sphere clusters. Although some attempts have been made to investigate the shape effect (e.g., Greenberg 1968; Rogers & Martin 1979; Draine 1988; etc.), the extensive calculations involved in all the methods do not readily permit extensive studies of the wavelength dependent interstellar extinction and polarization law. Until recently, only one attempt was made by Kim & Martin (1995a) to model the polarization law in terms of prolate/oblate particles. In our study we have modeled the interstellar dust grains as finite cylinders using the T-matrix method (Barber & Hill 1990) by simultaneously fitting *both* the extinction curve and the polarization law for the same particles. To provide both a comparison with our finite cylinder results and also to more readily consider a range of parameter variations

we have started with infinite cylinders, for simplicity. This will also be useful for comparing with many earlier results which used the infinite cylinder representation to give the polarization (Greenberg & Shah 1967; Hong & Greenberg 1980; Mathis 1986; etc.).

The dust compositions are discussed in Sect. 2. The optical constants of each dust component are presented in Sect. 3. In Sect. 4 we give a general description of the model calculations. The resultant extinction and polarization as well as comparisons with observations are presented in Sect. 5.1 and Sect. 5.2 for infinite and finite cylinders, respectively. The extensive modeling of the interstellar extinction curve follows in Sect. 6. We then discuss the polarization to extinction ratio and albedo in Sect. 7 and Sect. 8. Sect. 9 presents the cosmic abundance constraint followed by a summary in Sect. 10.

2. Dust composition

Interstellar spectral features play an important role in identifying interstellar dust compositions. It is well recognized that silicates are one of the major components of dust grains because of the presence of strong absorption and/or emission features at about 10 μm and 20 μm which are characteristic of the Si-O stretching and O-Si-O bending modes. In all existing dust models, silicates are a key component. But whether silicates are bare (Mathis, Rumpl & Nordsieck 1977, hereafter MRN; Draine & Lee 1984) or coated by organic refractory (Greenberg 1986), by hydrogenated amorphous carbon (HAC) (Duley, Jones & Williams 1989) or in other forms; e.g., composite (Mathis & Whiffen 1989) or fractal (Wright 1987) has been a key question. The presence of bare silicates in the abundance required by the MRN model appears to be precluded if one takes the dust destruction into account. Actually, the production rate of bare silicates by all possible astronomical sources is at least 10 times smaller than the destruction rate in the diffuse interstellar medium (Draine & Salpeter 1979a, 1979b; Greenberg 1986; McKee 1989; Jones et al. 1994). On the other hand, an organic refractory mantle on the silicates as cores could protect the cores from being destroyed by acting as an ablation shield (Greenberg 1986). The diffuse cloud 3.4 μm C-H stretching feature (Pendleton et al. 1994) also provides a test for the mantle material. While the organic refractory residues resulting from ultraviolet processing of interstellar ices provide a "fair" match to the 3.4 μm feature, it is not until such samples have undergone further ultraviolet processing as an analog of what occurs in the diffuse cloud medium that a remarkably close fit is achieved (Greenberg et al. 1995). In fact, it has been shown that such "second generation" residues provide a better match to the diffuse cloud 3.4 μm feature than all other assumed candidates; e.g., HAC, quenched carbonaceous condensate (QCC) etc. Finally, the fact that the silicate core-organic refractory mantle dust model provides an accurate match to the Becklin-Neugebauer object 10 μm and 20 μm polarization features (Greenberg & Li 1996a) while the other dust models based on bare silicate, composite dust grains, or silicates mantled by other materials all fail to reproduce the observations (see Greenberg & Li 1996a and references therein) also supports the idea that interstellar dust particles are silicate cores coated by organic refractory mantles.

The strongest feature in the extinction curve is, of course, the 2200 Å hump. Observations through various lines of sight show that the strength and width of the hump vary with environment while the hump peak position is quite invariant. Many candidates have been proposed as the hump carriers (for a recent review see Blanco et al. 1996), while no single one is generally accepted. Graphite was the earliest suggested and the widely adopted candidate in various dust models (Gilra 1972; MRN; Hong & Greenberg 1980; Draine & Lee 1984). However the hump peak position predicted from graphite particles is quite sensitive to the grain size, shape, and coatings (Gilra 1972; Greenberg & Chlewicki 1983; Draine 1988; Draine & Malhotra 1993) which is inconsistent with the observations. It was suggested that very small coated graphite particles ($a \leq 0.006\mu$m) could broaden the hump while keeping the hump peak constant (Mathis 1994). However, this is physically unlikely because the proposed particles are so small that temperature fluctuations will occur (Greenberg 1968) which will prevent the small graphite particles from acquiring a coating (Greenberg & Hong 1974a; Aannestad & Kenyon 1979)! Furthermore, it was noted by Greenberg & Hong (1974b) that if the very small particles as well as the large particles accrete mantles the value of $R_v = A_v/E(B-V)$ is *decreased* in molecular clouds. Another negative for graphite, is that the dust grains in circumstellar envelopes around carbon stars which are the major sources of the carbon component of interstellar dust particles are in amorphous form rather than graphitic (Jura 1986). It is difficult to understand how the original amorphous carbonaceous grains blown out from the star envelopes are processed to be highly anisotropic and evolve to the layer-lattice graphitic structures in interstellar space. It is more likely that the interstellar physical and chemical processes should make the carbonaceous grains even more highly disordered. The assumption of amorphous carbon is also unsuccessful because the predicted hump peak depends on the annealing degree and additionally the hump width is too weak (Bussoletti et al. 1987). Moreover, other attempts in terms of composite carbon (amorphous/glassy) particles (Blanco et al. 1996), QCC (Sakata et al. 1995), coals (Papoular et al. 1995) have all failed to match the hump width. Laboratory measurements made by Joblin et al. (1992) indicated that the hump could partially arise from the PAH's. This is controversial because, in the experimental results, the hump is always accompanied by some other bands which are not observed in the extinction curve. However, it may not be impossible that a mixture of large PAH's could be expected to smooth such features. A totally non-carbonaceous component, suggested by Duley, Jones & Williams (1989) is that the OH^- ion in silicates could produce the hump. The problem with this theory is that a large fraction of the silicate atoms are required to have an OH^- ion which is inconsistent with observations (Mathis 1996); e.g., along the sight line to VI Cyg #12 characteristic of the diffuse cloud, the ratio of the optical depth of the O-H stretching band to the the Si-O stretching band $\tau_{3.0\mu\mathrm{m}}/\tau_{9.7\mu\mathrm{m}}$ is less than 0.017 (Roche & Aitken 1984; Sandford et al. 1991; Pendleton et al. 1994). Although the hump

carrier is still quite uncertain, it is generally believed to be produced by small carbonaceous grains. In this work, we will not discuss the detailed optical properties of the hump particles but describe them by a Drude profile.

The carrier of the FUV extinction is also uncertain. It has been proposed to be very small graphite and/or silicate grains (Hong & Greenberg 1980; Sorrel 1989), or the long wavelength wing of a graphite resonance at 700 Å, or Polycyclic Aromatic Hydrocarbons (PAH) (Léger et al. 1989; Désert et al. 1990). The lack of correlation between the FUV extinction with the hump shown by Greenberg & Chlewicki (1983) rules out small graphite particles as the FUV contributor because they would produce both the hump feature and a substantial part of the FUV rising extinction. A factor against small silicate particles is that they would produce a feature in the FUV which is not observed in the extinction curve. It seems to us at this point that PAH's are the most likely (or the least unlikely) candidate. Although individual PAH's exhibit strong peaks in the UV/visual range, a mixture of many PAH's could produce a continuum absorption because the sharp features arising from individual PAH's differ from one another so that they could merge into a featureless continuum.

Thus in our model the interstellar dust particles are composed of three components — (1) large silicate core-organic refractory mantle particles which are responsible for the infrared and visual extinction and the entire polarization; (2) very small carbonaceous particles which are responsible for the hump; (3) PAH's which cause the FUV extinction. It is emphasized here that the term *unified model* refers to the fact that the polarization is produced by the *same* particles which are primarily responsible for the visual extinction. We realize that the uncertainties in the components responsible for the hump and the FUV extinction have yet to be resolved although it is our expectation that their sources are somehow related to having evolved from the organic refractory component of the large grains. A discussion of this is beyond the scope of this article but some suggestions have been made earlier (Greenberg et al. 1987a; de Groot et al. 1988; Jenniskens et al. 1993).

3. Optical constants

In order to study the interaction of light with dust particles, the knowledge of the optical constants of each component as a function of wavelength are required. Here the optical constants referred to are the complex indices of refraction, $m(\lambda) = m^{'}(\lambda) - i\,m^{''}(\lambda)$. In the following discussions, we first set the imaginary part $m^{''}(\lambda)$, and then derive the real part, $m^{'}(\lambda)$, from the Kramers-Kronig relation.

3.1. Silicates

A set of widely used optical constants of silicates are those of Draine & Lee (1984) which were derived from a synthesis of laboratory measurements and theoretical modeling of infrared spectral features. It is not surprising that the Draine & Lee silicates (1984) were unable to reproduce the interstellar silicate polarization because the optical constants in the infrared (around the silicate feature region) were derived on the basis of the bare silicate/graphite interstellar dust model which encounters fatal problems (Greenberg & Li 1996a). As shown in Greenberg & Li (1996a), the laboratory produced amorphous olivine $MgFeSiO_4$ (Dorschner et al. 1995) appears to be more representative of the astronomical silicates when taken as the core material in the silicate core-organic refractory mantle configuration. Due to the lack of FUV measurements for the amorphous olivine (Dorschner et al. 1995) which we favored, we adopt the optical constants of crystalline olivine measured by Huffman & Stapp (1973) for $\lambda \leq 0.3\,\mu$m. We note that there may be no significant differences in the FUV properties between crystalline and amorphous silicates because the absorption in the FUV is mainly due to the electronic transitions. This has been confirmed by the recent measurements of amorphous enstatite and forsterite by Scott & Duley (1996). The observational FUV polarization shows a featureless smooth behavior, while the sudden steep rise of $m^{''}(\lambda)$ in the FUV will result in a feature as pointed out by Kim & Martin (1995b), otherwise an extra population of very small particles is required and this is unreasonable since generally, smaller particles are more difficult to be aligned. Thus, following them, we shift the onset of absorption from 6.5 μm^{-1} to 7.5 μm^{-1} which is similar to that of the terrestrial rock, obsidian (Lamy 1978). For the range $0.3\,\mu\text{m} \leq \lambda \leq 2\,\mu$m, we have adopted the $m^{''}(\lambda)$ of Draine & Lee (1984) which is intermediate in absorptivity between that of Jones & Merrill (1976) and that of Rogers, Martin & Crabtree (1983) both of which were obtained by modeling the circumstellar dust emission or absorption. In addition, the optical constants derived for circumstellar silicate grains by the radiative transfer modeling of the IRAS data (David & Pégourié 1995) are close to those of Draine & Lee (1984) in the range $0.3\,\mu\text{m} \leq \lambda \leq 2\,\mu$m.

Finally, the imaginary part of the refraction index $m^{''}(\lambda)$ is joined smoothly to that of amorphous olivine (Dorschner et al. 1995). The real parts of the optical constants $m^{'}(\lambda)$ are calculated from $m^{''}(\lambda)$ by using the Kramers-Kronig relation. The resultant optical constants are shown in Fig. 1. It can be seen in Fig. 1 that, in the infrared, the differences in the real part of the refraction indices from those of Dorschner et al. (1995) to our modified ones are quite small.

3.2. Organic refractory

The idea of the presence of organic refractory as dust mantles can be traced to Greenberg et al. (1972) and has been confirmed both observationally and experimentally. Now it has been well established that an organic refractory mantle material results from the ultraviolet photoprocessing of ice mantles on silicate cores accreted in molecular clouds. These are further subjected to ultraviolet irradiation in diffuse clouds followed by repeated processing when cycling between diffuse clouds and molecular clouds (Greenberg 1982, 1986).

Since the optical constants of the astronomical organic refractory can not be measured directly, the laboratory created organic refractory residues from photoprocessed ice mixtures

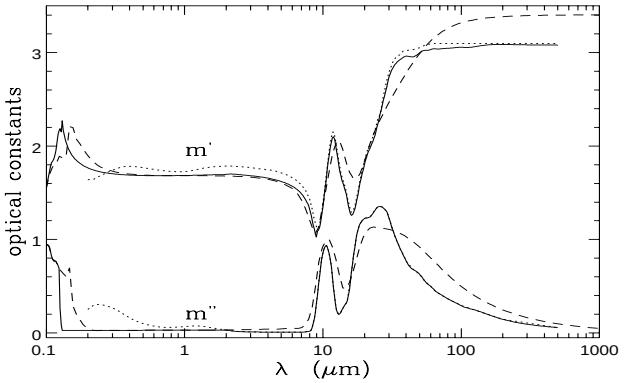

Fig. 1. Optical constants $m(\lambda) = m^{'}(\lambda) - i\,m^{''}(\lambda)$ of silicates. Dashed lines: synthetic "astronomical silicates" of Draine & Lee (1984); dotted lines: laboratory measured amorphous olivine (Dorschner et al. 1995); solid lines: modified amorphous olivine with the onset of FUV absorption shifted to shorter wavelength (this work, see text).

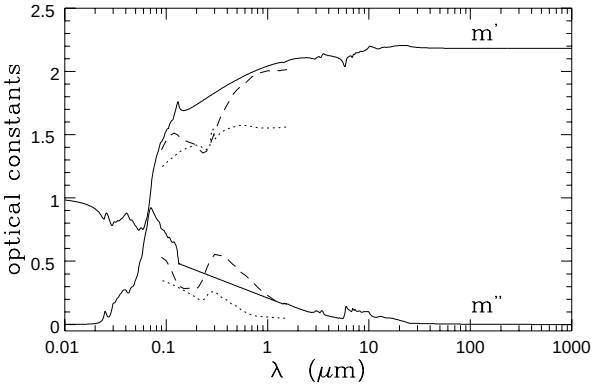

Fig. 2. Optical constants $m(\lambda) = m^{'}(\lambda) - i\,m^{''}(\lambda)$ of organic refractory (solid lines). Also shown are optical constants for processed organic residue (dotted lines) and for more heavily processed organic residue (dashed lines) measured by Jenniskens (1993).

have been used to measure the absorptivity and from this the optical constants are derived (Chlewicki 1985; Schutte 1988; Jenniskens 1993; etc). The problem is that the ultraviolet irradiation doses which the laboratory residues received are far less than those received by the dust mantles in interstellar space. So the optical constants of astronomical organic refractory may be different from those derived directly from laboratory data which are representative of grain mantles just emerging from molecular clouds ("first generation organic refractory"). In general, the more ultraviolet irradiation processed the grain mantles are the more complex and cross linked, and, therefore, more absorbing because they are more carbonized.

The EURECA samples (the "second generation" organic refractory residues) which resulted from exposing the laboratory created residues to the solar ultraviolet irradiation on the ERA (Exobiology Radiation Assembly) platform of the EURECA satellite for 6 months (Greenberg et al. 1995) made it possible to obtain greater processed laboratory organic residues. They are representative of grain mantles which have been subjected to ultraviolet photoprocessing in diffuse clouds. The EURECA samples give an accurate match to the 3.4 μm diffuse cloud feature (Greenberg et al. 1995; Pendleton et al. 1994) and are believed to provide a more reliable basis for deriving optical constants. However, one should bear in mind that although they more closely resemble the astronomical organic refractory, they are still only representative of the dust mantles which have undergone *one* evolutionary cycle. At the other extreme, the organic component of Murchison meteorite (Cronin & Pizzarello 1990; Ehrenfreund et al. 1991) could represent more greatly processed material than the astronomical organic refractory. The infrared optical constants derived as an intermediate between the EURECA samples and the organic component of the Murchison meteorite (Greenberg & Li 1996a), when used for the mantles of silicates, reproduced the Becklin-Neugebauer silicate polarization features at the 10 and 20 μm very well, in fact, better than any previous dust models. Moreover, the adopted optical constants, assuming a 0.1 μm core-mantle particle, give $\tau(3.4\mu\text{m})/\tau(9.7\mu\text{m}) \sim 0.08$ which is consistent with the observed Galactic center value within the observational uncertainties (Pendleton et al. 1994).

The organic refractory material is likely to exhibit strong absorption in the FUV, due to the electronic transitions. The optical constants in the FUV are taken to be the same as those of Chlewicki & Greenberg (1990) which were calculated as a collection of 40 Lorentz oscillators.

The optical constants in the near ultraviolet and visual are by far the poorest determined. See Jenniskens (1993) for a review on the evolutionary history of the adopted organic refractory constants in dust modeling. The visual optical constants were at one time assumed to be $m^{'} \sim 1.4$–1.5, $m^{''} \sim 0.05$ (Chlewicki 1985). In Chlewicki & Greenberg (1990) they adopted $m^{'} \sim 1.7, m^{''} \sim 0.15$ in the visual. The most recent dust modeling implied that $m^{''}$ could be as high as 0.4 (Xing 1993). Now with the availability of the FUV polarization observations and the measurements of laboratory organic residues (Jenniskens 1993) we are able to place further restraints. We construct a set of optical constants in the visual and ultraviolet on the basis of the following assumptions: (1) $m^{''}$ could be as high as $0.3 \sim 0.5$ which was required by theoretical modeling (Xing 1993) and was confirmed by laboratory measurements (Jenniskens 1993); (2) the fact that the interstellar polarization curves along various lines of sight are quite smooth implies that the optical constants in the ultraviolet and visual very probably have no strong resonance; (3) the imaginary part of the optical constant in the ultraviolet and visual is very likely decreasing with increasing wavelength rather than constant. The resulting optical constants of organic refractory are plotted in Fig. 2. We note again that the real part of the optical constants is calculated to be consistent with the Kramers-Kronig relation. In the end, the adopted optical constants will be justified by comparison of the model produced polarization and the observations.

3.3. Hump particles and FUV particles

As discussed in Sect. 2, the particles responsible for the 2200 Å hump were originally thought to be graphite but this has been strongly disputed for numerous reasons. Although they are not yet fully identified, it is generally believed that they are carbonaceous. In the hump region ($\lambda \leq 0.5\mu$m) we describe it by a Drude profile

$$\frac{Q_{abs}(\lambda,a)}{a} = \left(6.6\times10^4 x + \frac{1.92\times10^6 x^2}{(x^2-x_0^2)^2+\gamma^2x^2}\right)\ \mathrm{cm}^{-1} \quad (2)$$

where $x_0 = 4.6\,\mu\mathrm{m}^{-1}$, $\gamma = 1.0\,\mu\mathrm{m}^{-1}$ is the peak position and width of the Drude profile, respectively (Fitzpatrick & Massa 1986, Désert et al. 1990, Siebenmorgen & Krügel 1992); x is $\lambda^{-1}\mu\mathrm{m}^{-1}$; a is the size of the hump particle; and the peak absorption efficiency $Q_{abs}(\lambda,a)$ is normalized to match that of small graphite particles (Draine & Lee 1984) at the hump. For the rest of the wavelength region we use the graphite optical constants (Draine & Lee 1984) to calculate the absorption efficiencies by Mie theory.

The FUV particles, represented by PAH's, can not be described in terms of their complex indices of refraction, although some effort has been made in determining the optical constants of several PAH molecules in the laboratory (see, e.g., Allamandola et al. 1989). The absorption cross sections of PAH's are still uncertain, but some approximate results have been obtained both through laboratory and theoretical investigations (Léger et al. 1989; Joblin et al. 1992; Schutte et al. 1993; etc.). Following Désert et al. (1990), we adopt the absorption cross section of PAH's to be taken empirically by subtraction of the large particle and the hump component from the curvature of the extinction curve in the FUV and proportional to λ^{-2} in the visual. The FUV curvature in the diffuse cloud medium appears to be constant (Greenberg & Chlewicki 1983).

4. Model calculation description

The interstellar extinction and polarization result from the interaction between star light and interstellar dust grains. To model such an interaction, the knowledge of dust composition, shape, size, and alignment is required.

At first we confine ourselves to the large core-mantle particles which dominate the infrared and visual extinction and are assumed as the only contributor to the polarization. The composition has been strongly indicated to be exclusively silicate core-organic refractory mantle both of whose optical constants are given in Sect. 3. As to the shape, we first assume it to be an infinite cylinder and then model it in further detail by a more realistic shape — finite cylinder. It is noteworthy that, except for the fact that the infinite cylinder produces $\sim \lambda^{-3}$ dependent scattering in the long wavelength limit rather than $\sim \lambda^{-4}$ dependence as is the case for any finite size particles, and except that the infinite cylinder model overestimates the polarization-to-extinction ratio $(P/A)_v$, the infinite cylinder provides in many ways a reasonable representation of the interstellar polarization curve as shown by Greenberg (1968), Rogers & Martin (1979), Wolff et al. (1993) and, as we shall see later, in this work.

The size distribution is taken to be

$$n(a) = n_0\, exp\,[-5\,(\frac{a-a_c}{a_i})^q] \quad (3)$$

where a, a_c, a_i are the total radius of the core-mantle dust grain, the radius of the silicate core, the cut-off size of the distribution, respectively; the normalizing factor n_0 is $n_0 = 2\sqrt{5}/[\Gamma(\frac{1}{2})\,a_i]$ for $q = 2$. The average particle size is $< a >= a_c + 0.2522\,a_i$ (in case $q = 2$). Note that $n(a)$ is actually the distribution of the mantle thickness with the core size a_c kept constant for a given size distribution. Note also that we shall use a Gaussian rather than an e^{-a^3} type of distribution as has earlier been used by one of us (JMG) because it provides better fits to the observations by having relatively more large size particles.

For simplicity and because the differences between results for partial Davis-Greenstein alignment and perfect spinning alignment are not critical (Chlewicki & Greenberg 1990), we adopt perfect spinning alignment.

We thus calculate the extinction $A(\lambda)$ and linear polarization $P_l(\lambda)$, circular polarization $P_c(\lambda)$ cross sections as follows:

$$A_{cm}(\lambda) = 1.086\, n_{cm} \int_{a_c}^{\infty} \frac{2}{\pi} \int_0^{\pi/2} C_{geo}\, \frac{Re}{2}[\tilde{Q}_E(a,\lambda,\theta) + \tilde{Q}_H(a,\lambda,\theta)]\, n(a)\, d\theta\, da, \quad (4)$$

$$P_l(\lambda) = n_{cm} \int_{a_c}^{\infty} \frac{2}{\pi} \int_0^{\pi/2} C_{geo}\, \frac{Re}{2}[\tilde{Q}_E(a,\lambda,\theta) - \tilde{Q}_H(a,\lambda,\theta)]\, n(a)\, d\theta\, da, \quad (5)$$

$$P_c(\lambda) = n_{cm} \int_{a_c}^{\infty} \frac{2}{\pi} \int_0^{\pi/2} C_{geo}\, \frac{Re}{2}[\tilde{Q}_E(a,\lambda,\theta) - \tilde{Q}_H(a,\lambda,\theta)]\, \frac{Im}{2}[\tilde{Q}_E(a,\lambda,\theta) - \tilde{Q}_H(a,\lambda,\theta)] \times n(a)\, d\theta\, da, \quad (6)$$

where $\tilde{Q}_E$ and $\tilde{Q}_H$ are the complex extinction efficiencies for radiation polarized parallel or perpendicular to the particle symmetry axis; Re and Im denote the real and imaginary parts, respectively; θ is the incident angle of the radiation with respect to the symmetry axis (Greenberg 1968); C_{geo} is the geometrical cross section, and following Hong & Greenberg (1980), $C_{geo} = 4\,e\,a^2$ for a segment of infinite cylinder whose length is $2\,e\,a$ where e is the elongation (ratio of cylinder length to diameter); n_{cm} is the number density of the core-mantle particles. In effect, this is equivalent to using finite cylinders of constant elongation.

The cases for the hump particles and the PAH's are much simpler. The extinction cross sections contributed by the hump particles and the PAH's (both of which are assumed to be spherical) are

$$A_{hump}(\lambda) = n_{hump} \int_{a_-}^{a_+} \pi a^2 Q(a,\lambda) n(a) da \quad (7)$$

$$A_{PAH}(\lambda) = n_{PAH} \int_{a_-}^{a_+} C(a,\lambda) n(a) da \quad (8)$$

where n_{hump} and n_{PAH} are the number densities of the hump particles and PAH's, respectively; $C(a, \lambda)$ is the extinction cross section of PAH's. The size distributions for both hump particles and PAH's are assumed to be $n(a) \propto a^{-r}$ with a is in the range a_- to a_+. The parameters r, a_-, a_+ for the hump particles and PAH's differ from each other.

The total extinction contributed by all the dust components is then

$$A(\lambda) = A_{cm}(\lambda) + A_{hump}(\lambda) + A_{PAH}(\lambda). \quad (9)$$

Therefore there are altogether 12 free parameters in the model: (a_i, a_c, q, n_{cm}) for the core-mantle particles, (a_-, a_+, r, n_{hump}) for the hump particles and (a_-, a_+, r, n_{PAH}) for the PAH's. Since the interstellar polarization is exclusively contributed by the core-mantle particles, we need first constrain only (a_i, a_c, q) by fitting the interstellar polarization law, and then obtain the other 9 free parameters by matching the extinction curve.

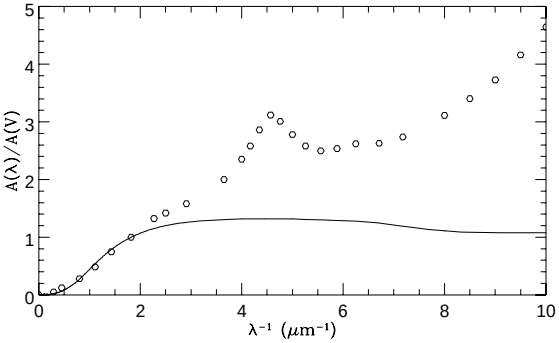

Fig. 3. Extinction produced by core-mantle infinite cylinders on the basis of the MGEMT with a size distribution of ($a_i = 0.08\,\mu$m, $a_c = 0.042\,\mu$m, $q = 2$) (solid line). Note that the core and the mantle have the same elongation in this approximation. Points represent the average interstellar extinction curve of the diffuse medium ($R_v \simeq 3.1$, Savage & Mathis 1979). Both are normalized to unity at the visual wavelength.

5. Interstellar polarization

5.1. Model results for the infinite cylinder

We shall consider first, for illustrative purpose as well as for comparison with much of the earlier work, the infinite cylinder representation of dust particles. Rigorous numerical solutions for arbitrarily oriented homogeneous infinite cylinders had been obtained by Lind & Greenberg (1966). Given the optical constants of the dust grain, one can calculate the extinction and polarization efficiencies per unit length by using the analytical forms given in Lind & Greenberg (1966). We first adopt the Maxwell-Garnett effective medium theory (hereafter MGEMT) to derive the effective optical constants of the core-mantle particles (Bohren & Huffman 1983) taking the silicate core to be the inclusion and the mantle to be the matrix. The validity of the homogeneity assumption by the MGEMT will be essentially confirmed by the exact solutions for the core-mantle infinite cylinder later in this section.

In the infinite cylinder case, we will only consider the polarization and the visual/IR extinction contributed by the core-mantle particles; i.e., we are not going to try to match the entire interstellar extinction curve. This will be deferred to the detailed modeling in terms of finite cylinder particles. Thus there are only 3 free parameters in our model calculations: (a_i, a_c, q) for the large core-mantle particles. We have carried out calculations for a grid of parameters (a_i, a_c, q) and find the best match to both the visual/IR extinction and the polarization is provided by core-mantle particles with a size distribution of $a_i = 0.08\,\mu$m, $a_c = 0.042\,\mu$m, $q = 2$. We note that the match to the optical polarization curve can also be achieved with a cubic exponential size distribution ($q = 3$) by adjusting a_i and a_c. The reason why we chose $q = 2$ is that it works better for finite size particles in fitting the observed near infrared polarization where relatively more large particles are required for the longer wavelength polarization. The theoretical extinction curve, as shown in Fig. 3, increases from the IR to the visual with a slope change at $\lambda^{-1} \sim 0.8\,\mu\text{m}^{-1}$, after which it saturates at $\lambda^{-1} \sim 3.0\,\mu\text{m}^{-1}$ and ultimately becomes rather flat. In fact the drop in the extinction at $\lambda^{-1} \sim 10\,\mu\text{m}^{-1}$ from the maximum is only about 20%. It is evident in Fig. 3 that the core-mantle particles dominate the visual/IR extinction. Fig. 4 shows the calculated linear polarization (linear dichroism) as well as the observations represented by the Serkowski empirical law for the diffuse medium. In the near infrared ($\lambda > 1.64\,\mu$m), a power law $P(\lambda) \propto \lambda^{-1.8}$ is also plotted to approximate the NIR polarization observations. The match of the calculations to the observations is quite good over a wide wavelength range, with the predicted value a little less in the FUV ($\lambda^{-1} > 7\,\mu\text{m}^{-1}$) although well within the observational uncertainties. Fig. 4 also illustrates that, in the NIR, the theoretical polarization is a little higher than the Serkowski law, but still a little bit lower than the power law. The circular polarization (the product of the linear birefringence and dichroism) is presented in the inset panel in Fig. 4. Quite evidently, the wavelength λ_c at which the theoretical circular polarization changes its sign is very close to the wavelength λ_{max} at which the linear polarization peaks which is consistent with the observations (Martin & Angel 1976; McMillan & Tapia 1977). This is not unexpected. As shown in Chlewicki & Greenberg (1990), the $\lambda_c = \lambda_{max}$ relationship would always automatically be obtained if the adopted optical constants satisfy the Kramers-Kronig relation.

We should keep in mind that the above results were obtained on the basis of the Maxwell-Garnett effective medium theory (MGEMT), while the MGEMT is only applicable to spherical particles with the size parameters of their elements (the matrix and the inclusions) smaller than the wavelength of the incident electromagnetic field. However, in our dust model, the particles are assumed to be nonspherical; moreover, in the FUV, the particle constituents (in particular, the mantles) are certainly not always smaller than the wavelength. In order to justify the validity of the MGEMT adopted in our model calculations, we first discuss the size effects in terms of spherical core-mantle

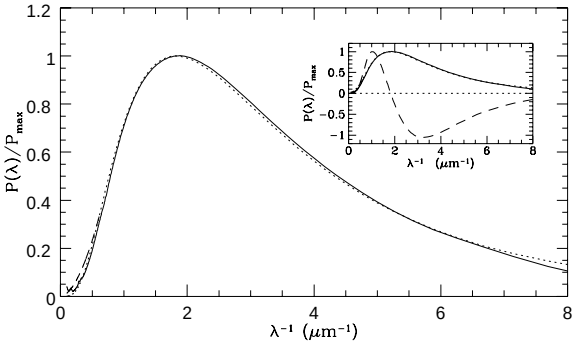

Fig. 4. Linear polarization provided by the same infinite cylinder particles as in Fig. 3 (solid). Also shown is the "observational interstellar polarization" represented by the Serkowski law ($\lambda_{max} \simeq 0.55\,\mu$m) (dotted) and a power law $P(\lambda) \propto \lambda^{-1.8}$ in the NIR (dashed). Both are normalized to the peak polarization (P_{max}). The inset plots circular polarization (dashed line) as well as theoretical linear polarization (solid) and the Serkowski law (dotted).

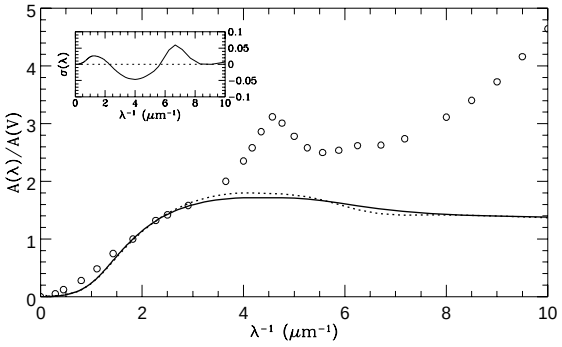

Fig. 5. Extinction by spherical core-mantle particles having a size distribution with $a_i = 0.11\,\mu$m, $a_c = 0.07\,\mu$m, $q = 2$ and an average size 0.1 μm. Solid line corresponds to the homogeneous sphere Mie solution based on the MGEMT ($A_{MG}(\lambda)$). Dotted line corresponds to the exact solution for coated spheres ($A_{CM}(\lambda)$). Both of them are normalized to $A_{MG}(v)$. The upper-left insert in the figure shows the errors $\sigma(\lambda)$ introduced by the MGEMT approximation, $\sigma(\lambda) = (A_{MG}(\lambda) - A_{CM}(\lambda))/A_{CM}(\lambda)$.

particles, then we investigate the shape effects by comparing the results for the exact solutions of coated infinite cylinders with those for the MGEMT.

We have carried out calculations for spherical core-mantle particles on the basis of (1) the homogeneous representation plus the MGEMT; and (2) the exact solutions. The best fits to the interstellar extinction are, for *both*, provided by the particles with a size distribution of $a_i = 0.11\,\mu$m, $a_c = 0.070\,\mu$m, $q = 2$ which leads to a mantle to core volume ratio $v_m/v_c \approx 2.12$. Fig. 5 presents the model results for both cases where for comparison, both of them are normalized at the visual extinction cross section of the MGEMT case. They are clearly very close. Actually, up to $\lambda^{-1} \simeq 2.8\,\mu\text{m}^{-1}$, they are almost identical. Some discrepancies occur in the range $3\,\mu\text{m}^{-1} < \lambda^{-1} < 8\,\mu\text{m}^{-1}$ with the most prominent discrepancies at $\lambda^{-1} \simeq 4\,\mu\text{m}^{-1}$ and $\lambda^{-1} \simeq 7\,\mu\text{m}^{-1}$. The former results from the fact that the extinction produced by the dust particles peaks at $\lambda^{-1} \simeq 4\,\mu\text{m}^{-1}$; the latter is due to the strong resonance in the optical constants of the silicate particles in that wavelength range. However, as shown in the insert in Fig. 5, the largest discrepancy $\sigma(\lambda)$, defined as $(A_{MG}(\lambda) - A_{CM}(\lambda))/A_{CM}(\lambda)$, is only 7% and $\sigma(v) \simeq 1.8\%$ ($A_{MG}(\lambda)$ is the extinction cross section for the MGEMT; $A_{CM}(\lambda)$ for the exact solution). Thus we conclude that the differences between the MGEMT and the exact solution for spherical core-mantle particles are certainly not critical, even though all of the dust grains in the distribution have a size parameter $x = 2\pi\, a/\lambda > 1$ in the FUV.

We have also modeled the core-mantle particles using the exact solutions for coated infinite cylinders (Greenberg 1968; Shah 1970). The modeling procedure is the same as the MGEMT one except the exact solutions are adopted instead of the homogeneous infinite cylinder solutions plus the MGEMT. The best match to the observations are given by: $a_i = 0.104\,\mu$m, $a_c = 0.030\,\mu$m, $q = 2$. Comparing the MGEMT model results shown in Fig. 3 and Fig. 4 with those in Fig. 6 and Fig. 7, one finds that the differences are negligible. In addition to that, the fact

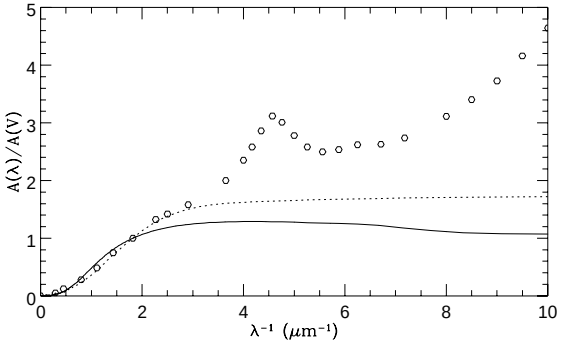

Fig. 6. Extinction by core-mantle infinite cylinders (solid line) with a size distribution of $a_i = 0.104\,\mu$m, $a_c = 0.030\,\mu$m, $q = 2$ in terms of exact solution. Note that both the core and the mantle have the same length in this solution. The dotted line corresponds to the extinction by core-mantle finite cylinders (see Sect. 5.2) on the basis of the MGEMT. The grain size distribution is given by: $a_i = 0.066\,\mu$m, $a_c = 0.070\,\mu$m, $q = 2$. The finite cylinder curve beyond $\lambda^{-1} = 4\,\mu\text{m}^{-1}$ where further calculations are limited by computer capability is extrapolated from those shortward of $4\,\mu\text{m}^{-1}$.

that in both cases, the volume ratios of the mantle to the core ($v_m/v_c \approx 2.87$ for the MGEMT and $v_m/v_c \approx 2.94$ for the other) are almost the same further convinces us of the validity of the MGEMT approximation adopted in the model calculations. We note that the differences in the parameters (a_i, a_c) are mainly due to the different cylinder length : in the homogeneous plus MGEMT case, the mantle length is longer than the core length since the core and the mantle have the same elongation; while in the exact core-mantle solutions, both the core and the mantle have the same length. We conclude that, for the current purpose, the MGEMT can also be applied to nonspherical core-mantle particles.

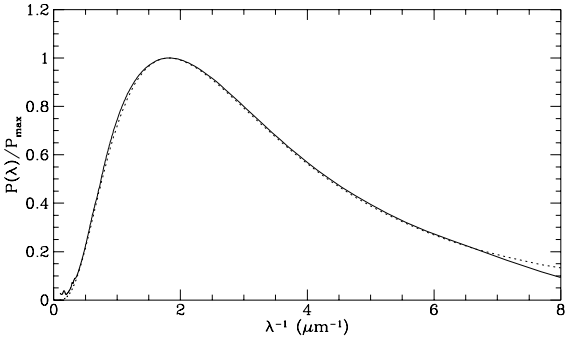

Fig. 7. Linear polarization produced by the same particles (infinite cylinders) as in Fig. 6. Dotted line is the Serkowski law.

Another widely used effective medium theory is the so-called Bruggeman rule (hereafter BEMT; Bohren & Huffman 1983). The main difference between the BEMT and the MGEMT is that, in the BEMT, there is no specified matrix or inclusion, in other words, the mixtures are treated symmetrically. We have also performed calculations on the basis of BEMT for the homogeneous infinite cylinder. We found there is only a minor difference when comparing with those based on the MGEMT. We have compared the effective refraction indices obtained using the BEMT or the MGEMT and found that significant deviations only occur in the strong resonance regions; e.g., around the silicate 10 μm and 20 μm bands, while the deviations are negligible in other regions where we are interested; i.e., the continuum. Even in the strong resonant region, the maximum of $(m'_{MG}-m'_B)/(m'_{MG}+m'_B)$ is only 2%, the maximum of $(m''_{MG}-m''_B)/(m''_{MG}+m''_B)$ may be as high as 8%.

Thus we conclude that, for dust extinction and polarization modeling, the core-mantle particles can be represented as homogeneous on the basis of the MGEMT. Actually, since core-mantle infinite cylinders are relatively simple to calculate, the MGEMT is not really required for extensive modeling and parameter variation.

5.2. Model results for the finite cylinder

The real interstellar dust particles are certainly not spheres or infinite cylinders. In fact, they are more likely to be irregularly shaped. Unfortunately, the problem of light scattering by irregular particles is so complicated that there are only a few approaches to date; i.e., DDA (Purcell & Pennypacker 1972; Draine 1988) and VIEF (Hage & Greenberg 1990) which are able to treat such problems. The fact that the DDA method as well as the VIEF method are very time-consuming places practical constraints on an extensive investigation of the interstellar extinction and polarization. The requirement of realistic shape and the limitation of the computer resources (CPU time, RAM storage, etc.) lead to a compromise: axisymmetrical particles are taken to represent the interstellar grains. Spheroids and finite cylinders are the two typical axisymmetrical particles which have been used. In this section we are going to model the interstellar grains as finite cylinders. The spheroid case has been treated by Kim & Martin (1995a) in terms of the bare silicate/graphite model. In the future we will consider modeling the interstellar grains as silicate core-organic refractory mantle spheroids.

Although no analytical solution exists for the light scattering problem by finite cylinders, numerical approaches have been extensively developed, amongst which the T-matrix method (Barber & Yeh 1975) is probably the most stable and presently the most actively used approach to solve the finite cylinder problem (Barber & Hill 1990; Xing 1993; Kuik et al. 1994). In the T-matrix method, both the incident (known) and the scattered electric fields (unknown) are expanded as vector spherical harmonic functions. Those expansion coefficients are connected by the transition matrix ("T-matrix"). Once the T-matrix is solved, one can derive the expansion coefficients of the scattered field and from which the optical properties can be obtained. The recent development and release of the Fortran codes of the T-matrix method made by Barber & Hill (1990) provided an opportunity to model the interstellar grains as finite cylinders. We use their codes to carry out the calculations. For further information about the method and the codes we refer to Barber & Hill (1990). We note that even the present T-matrix method is only able to treat homogeneous particles, so we represent the core-mantle finite cylinders by homogeneous finite cylinders by calculating the average dielectric functions through the MGEMT. The validity of the MGEMT for infinite cylinders and particularly for spheres has been shown in Sect. 5.1, so that one can expect that it may also work for finite cylinders.

Theoretically, the electric fields should be expanded as an infinite number of terms. In practice, only a finite number of terms are required to reach convergency with acceptable accuracy. The required number of terms is determined by the convergency test. For larger sizes, larger elongations, higher indices of refraction, more terms are needed to reach convergency. The computer resources restrict us in applying calculations to large size parameters. In our case, the code can go no further than $\lambda^{-1} \simeq 4\,\mu\mathrm{m}^{-1}$ with reliable accuracy.

We have calculated a grid of combinations of (a_i, a_c, q) for elongation e = 2. We did not treat the cases for e = 1 and e = 3 as extensively as the case for e = 2, because, for e = 3, convergence occurs at size parameters too small to be useful for dust modeling; while the e = 1 case is not a good approximation for elongated dust particles. The best match to the observations of polarization is provided by a size distribution of (a_i = 0.066 μm, a_c = 0.070 μm, q = 2). Other combinations of (a_i, a_c) may also be able to give a good fit to the polarization, but they can not satisfy the cosmic abundance constraints (see Sect. 9) as good as this. We have also tried the cases for q = 3 and q = 1.5. The reason that the q = 2 case is better than that for q = 3 is that, in the q = 2 size distribution, large particles make a relatively greater contribution than in the q = 3 distribution as required to match the near IR polarization. The calculated extinction curve is also shown in Fig. 6. It is similar to that for infinite cylinders except that its saturation begins at a slightly larger λ^{-1} and it produces more extinction in the $\lambda^{-1} \sim 2$ –

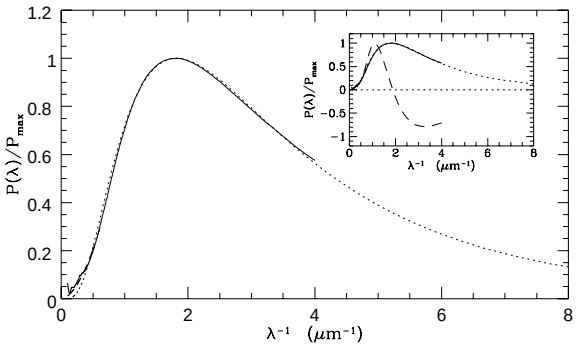

Fig. 8. Linear polarization (solid line) given by the same finite cylinder particles as in Fig. 6. Dotted line is responsible for the Serkowski law. Dashed line is the power law for the near infrared. The inset shows the theoretical circular polarization (dashed), linear polarization (solid) and Serkowski law (dotted).

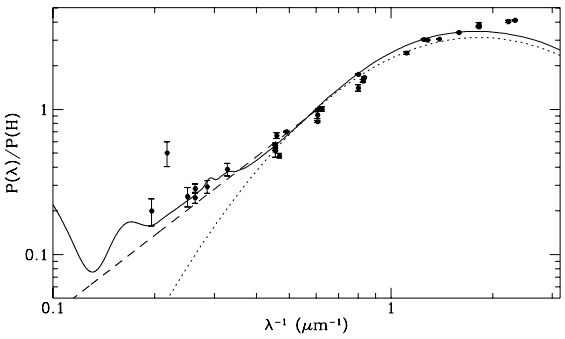

Fig. 9. Near infrared polarization for: 1) model results predicted by the finite cylinder particles (solid line); 2) observations for typical diffuse interstellar medium along the line of sight to VI Cyg #12 (points; Martin et al. 1992 and references therein); 3) Serkowski law (dotted); 4) power law $P(\lambda) \propto \lambda^{-\beta}$ where $\beta \simeq 1.8 \pm 0.2$. All are normalized at H band ($\lambda \approx 1.65\,\mu$m).

$4\,\mu\mathrm{m}^{-1}$ region. The extinction curve beyond $\lambda^{-1} = 4\,\mu\mathrm{m}^{-1}$ is obtained from the extrapolation of the calculated curve for $\lambda^{-1} \leq 4\,\mu\mathrm{m}^{-1}$. It may introduce some uncertainties in the small particle populations but should not greatly affect any of the basic constraint considerations. The linear polarization is shown in Fig. 8. It can be seen that in the wavelength range for which calculations are done, the model results reproduce the observations very well. Similar to the infinite cylinder model, the circular polarization predicted from the finite cylinder is also plotted in Fig. 8 as an inset. Evidently, $\lambda_c \simeq \lambda_{max}$ is also the case for the finite cylinder model. It further supports the conclusion of Chlewicki & Greenberg (1990) that $\lambda_c \simeq \lambda_{max}$ is always satisfied as long as the optical constants satisfy the Kramers-Kronig relation, no matter what shape or how absorbing the particles are.

The near infrared polarization has recently received greater interest and indicates the great advantage of the finite cylinder model since although the infinite cylinder model is also able to fit the visual and UV polarization (Hong & Greenberg 1980; Kim & Martin 1994; Sect. 5.1 of this work; etc.) it is not able to fit the NIR. Recent observations show that the NIR polarization ($\lambda \sim 2$ – 5μm) is in excess of that extrapolated from the Serkowski law (Martin & Whittet 1990; Martin et al. 1992 and references therein). The attempts to reproduce the NIR polarization by infinite cylinders have been unsuccessful (Kim & Martin 1994; Sect. 5.1 of this work). However, our model results for finite cylinders are quite good. Fig. 9 compares the NIR polarizations of the model prediction, the Serkowski law and a power law approximation which is thought to be representative of the observations of the NIR polarization. Also plotted are the observational data for VI Cyg #12. We recall that, although the optical polarization of VI Cyg #12 peaks at $\lambda_{max} \simeq 0.5\,\mu$m rather than $\lambda_{max} \simeq 0.55\,\mu$m characteristic of the diffuse medium, the power index β (see Sect. 1) of the NIR polarization power law is independent of λ_{max} (Martin et al. 1992). Thus the VI Cyg #12 observations provide a good representation of the interstellar NIR polarization. It is clear in Fig. 9 that our model is quite successful in reproducing the NIR observations. The features at $\lambda \sim 6\,\mu$m and $\sim 10\,\mu$m are due to organic refractory and silicates, respectively. It is worth noting that spheroids are also shown to provide a better match to the NIR polarization than infinite cylinders (Kim & Martin 1995a). It is also noteworthy that although the cubic exponential size distribution ($q = 3$) infinite cylinder model is also able to reproduce the optical/UV polarization, only the $q = 2$ size distribution in the finite cylinder model is able to provide a good fit to the NIR polarization, because the larger particles are more responsible for the NIR polarization ($a \sim \lambda/2\,\pi\,(m^{'} - 1)$, Greenberg 1968). In this respect, our results are consistent with the requirement of a secondary large size peak in the mass distribution of the spheroid model (Kim & Martin 1995a).

6. Interstellar extinction

We extend the match of the model to the full interstellar extinction curve with combinations of the core-mantle finite cylinder particles, the hump particles and the PAH's. In the fitting, there are altogether 12 free parameters: (a_i, a_c, q, n_{cm}) for the core-mantle particles; (a_-, a_+, r, n_{hump}) for the hump particles; (a_-, a_+, r, n_{PAH}) for the PAH's. Three parameters (a_i, a_c, q) for the core-mantle particles have already been determined in Sect. 5.2, and by adjusting the remaining 9 parameters, a good fit to the extinction curve can be obtained. The value of the total to selective extinction ratio for the core-mantle particles alone is $R_v = 3.5$. As will appear next, the addition of the contribution of small particles leads to $R_v = 3.1$. It is interesting to note that any reduction in the hump particles (normally by accretion on the core-mantle particles) automatically increases the value of R_v in addition to the large particle's size increase effect.

With the fixed parameters of the core-mantle particles determined in Sect. 5.2, we explore the contributions by the hump particles and the PAH's. The whole interstellar extinction curve is fitted by the size distributions of ($a_- = 15$ Å, $a_+ = 120$ Å, $r = 3$) for the hump particles and ($a_- = 6$ Å, $a_+ = 15$ Å,

$r = 3$) for the PAH's. The resultant theoretical extinction curve is given by the sum of three components: core-mantle particles with $n_{cm}/n_H \simeq 3.89 \times 10^{-13}$; hump particles with $n_{hump}/n_{cm} \simeq 5.22 \times 10^3$ and PAH's with $n_{PAH}/n_{cm} \simeq 7.99 \times 10^5$. We adopt $N_H/A_v = 1.9 \times 10^{21}\,\mathrm{cm}^{-2}$ (Bohlin et al. 1978). The mass ratios are $m_{hump}/m_{cm} \simeq 0.11$ and $m_{PAH}/m_{cm} \simeq 0.12$. So that the large particles account for almost 80% of the total mass (Greenberg & Li 1995; Block et al. 1994). The relevant parameters are summarized in Table 1. We note that the size distribution parameters for the hump particles and PAH's are more flexible than for the core-mantle particles because the extinction efficiencies are not very sensitive to the size in the size ranges considered, so that the a_-, a_+ are not critical.

Fig. 10 shows the comparison of the observed interstellar extinction curve with the theoretical result. Also plotted are the individual contributions of the three dust components. The mean interstellar extinction curve is represented by the data from Savage & Mathis (1979). Our model results match the observations quite well except in the 6.3 $\mu\mathrm{m}^{-1}$ region. However, as pointed out by Massa et al. (1983), this structure is an artifact feature due to the mismatch error across the CIV feature which produces such a spurious elevation in the extinction curve at 6.3 $\mu\mathrm{m}^{-1}$. Further investigation, especially high resolution observations in this region are needed.

The absorption and polarization properties in the infrared, in particular, around the 10 μm and 20 μm silicate resonance, are also essential to constrain dust models. The left-top panel in Fig. 10 illustrates the predicted infrared extinction curve in which the most prominent features are the silicate bands. The calculated silicate feature strength above the continuum is $\tau_{9.7\mu\mathrm{m}}/\mathrm{A}_v \simeq 0.037$ which is lower than the observational result of $\tau_{9.7\mu\mathrm{m}}/\mathrm{A}_v \simeq 0.054$ (Roche & Aitken 1984). This discrepancy may result from the underestimation of the silicate band strength (in other words, the real astronomical silicate may have a greater band strength than the laboratory analog). Another possibility is that the observed $\tau_{9.7\mu\mathrm{m}}/\mathrm{A}_v$ (0.054) may have been overestimated due to the presence of the PAH 7.7 μm emission (Cohen et al. 1989) which effectively raises the continuum. With regard to the infrared polarization, the core-mantle model gives a quite good match to the interstellar silicate polarization observations (see Greenberg & Li 1996a).

Exposed to the interstellar radiation field, the grains absorb photons in UV/visual and radiate in infrared. Thus the IR emission provides further tests of dust models. As shown by Greenberg & Li (1996b), the trimodal dust model provides a reasonable fit to the IRAS and COBE observations. We have recalculated the IR emission in terms of the size distributions derived in this work and the results are in good agreement with the observations. We should note that while the infrared (continuum) emission does not critically define the "details" of the dust size distribution it does seem to require a trimodal distribution as provided by our model; namely, large particles (responsible for the FIR emission at $\lambda \geq 100\,\mu$m) and two populations of very small particles undergoing temperature fluctuating (responsible for the near and mid infrared emission).

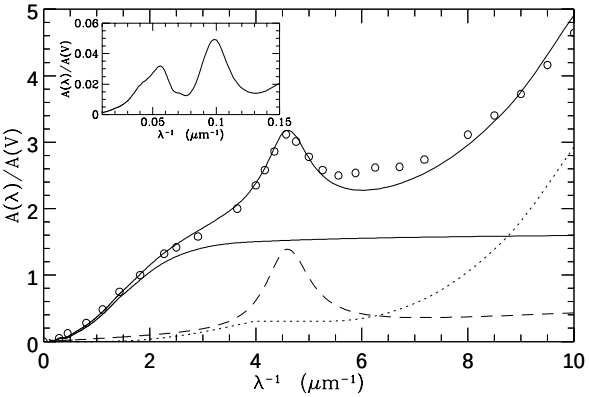

Fig. 10. Fits to the interstellar extinction curve (points; Savage & Mathis 1979). Model results (thick solid) are the sum of three dust components: 1) finite cylinders (thin solid); 2) hump particles (dashed); 3) PAH's (dotted). The inset is the infrared extinction curve.

7. The polarization to extinction ratio

Observations have well established that the ratio of the linear polarization to the extinction at visual $(P/A)_v \leq 0.03$. This criterion is related to both the alignment efficiency and the scattering properties of the dust particles. In spite of the fact that this is an *upper* limit, it places further constraints on dust models and even rules out some models because this *upper* limit should be *reachable* under ideal conditions. In Fig. 11 are shown the polarization to extinction (including the contributions of the hump particles and the PAH's) ratios versus wavenumber (λ^{-1}) for both the finite cylinder model and the infinite cylinder model. The predicted $(P/A)_v$ for the finite cylinder model is ~ 0.09 and about twice as high for the infinite cylinder model (~ 0.22) both of which are much higher than the observational criterion. Since our results were obtained for perfect spinning alignment and a magnetic field perpendicular to the line of sight, the excess of $(P/A)_v$ allows that in a real interstellar regime, the grain alignment need not be ideal; e.g., magnetic field not perpendicular to the line of sight. The polarization to extinction ratio in the mid-infrared and far infrared for the finite cylinder model is presented in the upper-right little box in Fig. 11. It shows a resonant structure in the silicate feature region and approaches a constant value (≈ 0.37) in the far infrared.

The conclusions which we can draw from Fig. 11 are: (1) the core-mantle dust model has no difficulty in satisfying the $(P/A)_v$ criterion; (2) the finite size particles produce a $(P/A)_v \sim 1/2$ of that of infinite cylinders as already pointed out decades ago (Greenberg 1968).

It is of interest to question whether all grain models readily satisfy the $(P/A)_v$ criterion. For example, in the bare silicate/graphite model (MRN; Draine & Lee 1984), the extinction is the sum of the extinctions A_{si} and A_{gra} produced by the silicates and the graphite particles, respectively, while the polarization is produced by the silicates P_{si} *alone* since the graphite

Table 1. Sizes and numbers of each dust component in the diffuse cloud determined from the finite cylinder model ($A_v/N_H \simeq 5.3 \times 10^{-22}$ mag cm^2).

	core-mantle	hump	PAH
grain	$n(a) \sim exp\,[-5\,(\frac{a-a_c}{a_i})^q]$	$n(a) \sim a^{-r}$	$n(a) \sim a^{-r}$
size	a_c=0.070 μm, a_i=0.066 μm, q = 2	$a \in$ [15, 120] Å, r = 3	$a \in$ [6, 15] Å, r = 3
n_d/n_H	3.89×10^{-13}	2.03×10^{-9}	3.11×10^{-7}
n_d/n_{cm}	1.00	5.22×10^{3}	7.99×10^{5}
m_d/m_{cm}	1.00	0.11	0.12

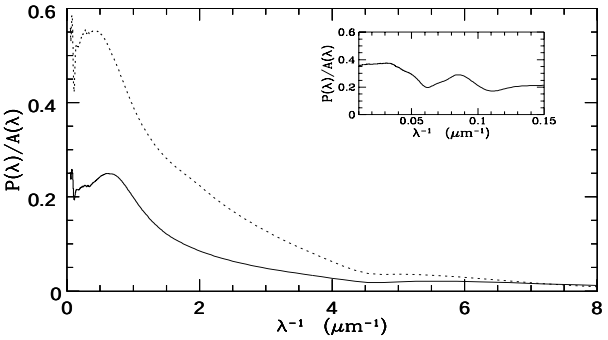

Fig. 11. Theoretical polarization to extinction ratio for finite cylinder model (solid line) and for infinite cylinder model (dotted line). The polarization is produced by the large grains (core-mantle particles) alone while the extinction includes the contributions of all three dust components. The inserted box shows the polarization to extinction ratio in the mid-infrared and far infrared for the finite cylinder model.

grains are very difficult to be aligned (Greenberg 1968). The $(P/A)_v$ is then *diluted* according to

$$\left(\frac{P}{A}\right)_v = \frac{P_{si}(v)}{A_{si}(v)+A_{gra}(v)} = \frac{P_{si}(v)/A_{si}(v)}{1+A_{gra}(v)/A_{si}(v)}. \quad (10)$$

For perfect spinning *infinite* cylinder silicates, $P_{si}(v)/A_{si}(v)$ is shown to be ≈ 0.134 (Mathis 1986). Draine & Lee (1984) obtained $A_{gra}/A_{si} \approx 0.7/0.3$ in terms of *spherical* particles. Thus we get $(P/A)_v \approx 0.04$. But since, as shown in Fig. 11, the $(P/A)_v$ for the *finite* size particles is only $\sim 1/2$ of that of infinite cylinders, we expect that the maximum polarization to extinction ratio in the visual is $(P/A)_v \approx 0.02$. Thus the silicate/graphite model encounters a problem in producing the observed $(P/A)_v$. However, the adopted $P_{si}(v)/A_{si}(v)$ and A_{gra}/A_{si} values were not derived from the same modeling (actually, they were obtained in terms of different shape and size distributions etc.), so the actual result may be different. A detailed discussion on the $(P/A)_v$ constraints in terms of simultaneous fitting of both the extinction and the polarization observations for the silicate/graphite model is in progress but preliminary results do not show a sufficient improvement in satisfying the $(P/A)_v$ requirement.

A suggestion which attempts to remove this dilemma is that the large grains are composites of various sorts (Mathis & Whiffen 1989; Mathis 1996) so that the polarization and the principal visual extinction are both produced by such particles. It is arbitrarily assumed that these composite particles are nonspherical enough to produce significant polarization when aligned. The initial model (Mathis & Whiffen 1989) did not produce a good match to the interstellar polarization (see also Wolff et al. 1993). The new composite model (Mathis 1996) has not yet been subjected to a calculation for polarization but, let us grant for the moment that this can be done successfully. Insofar as alignment is concerned one would have to invoke suprathermal spin-up in order to achieve an adequate polarization to extinction ratio. It is the spin-up which leads to the most crucial constraint on these aggregate particles.

According to Purcell (1979) and Spitzer & Mc Glynn (1979) the spin-up to angular velocities as great as $10^9\ s^{-1}$ will occur unless limited by some sort of process such as accretion. With no accretion, long lived spin-up is expected and in diffuse clouds, where no ices are observed, we can assume that accretion is negligible so that maximum angular speeds are approached.

The tensile stress induced in a spherical particle of mass m, radius r and angular velocity ω is

$$S \simeq \frac{m\,\omega^2\,r}{\pi\,r^2} = \frac{4}{3}\,\rho\,r^2\,\omega^2 \quad (11)$$

If we consider the mean size of the aggregates proposed by Mathis & Whiffen (1989) as representative of interstellar dust in the diffuse cloud medium we should use $\bar{r} \approx 0.4\mu$m and $\rho = \rho_0\,(1-P)$ with fully compacted density $\rho_0 \simeq 2$ g cm^{-3} and a porosity $P = 0.8$ which implies a vacuum of 80%. Thus we may write

$$S \simeq 4.3 \times 10^9 \left(\frac{\rho_0}{2\ \mathrm{g\,cm^{-3}}}\right)(1-P)\left(\frac{r}{0.4\,\mu\mathrm{m}}\right)^2 \times \left(\frac{\omega}{10^9\ s^{-1}}\right)^2\ \mathrm{dyn\,cm^{-2}}. \quad (12)$$

The tensile strength of an aggregate of small particles has been calculated to be (Greenberg, Mizutani & Yamamoto 1995)

$$T_{ag} = 3\,\beta\,(1-P)\,\bar{E}\,/2a^2h \quad (13)$$

where β = mean number of contact points per particle between particles ($1 \le \beta \le 10$), $\bar{E}$ = mean intermolecular interaction energy at the contact surfaces, a = mean particle size in the aggregate, h = mean intermolecular distance at the contact surfaces. We shall assume that $\bar{E}$ is essentially due to van der Waals forces so that $E = \alpha\,10^{-3}\,eV$, $h = 0.3$ nm. The mean

particle size, following Mathis & Whiffen (1989), is taken as $a = 5\,\mathrm{nm}$ (0.005 μm). The tensile strength of such an aggregate is then

$$T_{ag} = 1.6\times10^{6}\left(\frac{\beta}{5}\right)(1-P)\left(\frac{\bar{E}}{10^{-3}\,eV}\right)\left(\frac{\alpha}{1}\right)\left(\frac{a}{5\,\mathrm{nm}}\right)^{-2} \times\left(\frac{h}{0.3\,\mathrm{nm}}\right)^{-1}\ \mathrm{dyn\,cm^{-2}} \quad (14)$$

Thus the stress to strength ratio for the spinning aggregate is

$$\frac{S}{T_{ag}} \simeq \frac{4.3\times10^{9}}{1.6\times10^{6}} = 2.7\times10^{3} \gg 1, \quad (15)$$

so that, even for incomplete spin-up to $\omega = 10^{8}\ s^{-1}$, all grains in the Mathis & Whiffen (1989) size distribution with $r \geq 0.08\mu$m should be blown apart. In view of the fact that the maximum grain size needed in the $a^{-3.5}$ distribution to produce the observed extinction or polarization, according to Mathis & Whiffen (1989), is $a_{max} = 0.9\mu$m, we see that there would be a severe deficit of all the large grains ($0.08 \leq a \leq 0.9\mu$m destroyed) and that neither the wavelength dependence of extinction nor polarization could possibly be matched (Greenberg & Li 1996c).

An equivalent calculation for the Mathis (1996) aggregate model leads to

$$\frac{S}{T_{ag}} \simeq 175\left(\frac{\rho_0}{2.8\,\mathrm{g\,cm^{-3}}}\right)(1-P)\left(\frac{r}{0.16\,\mu\mathrm{m}}\right)^{2}\left(\frac{\omega}{10^{9}\,s^{-1}}\right)^{2} \times\left(\frac{5}{\beta}\right)\left(\frac{\bar{E}}{10^{-3}\,eV}\right)\left(\frac{1}{\alpha}\right)\left(\frac{a}{2\,\mathrm{nm}}\right)^{2}\left(\frac{h}{0.3\,\mathrm{nm}}\right) \quad (16)$$

where the aggregates, with $P = 0.45$, are less porous than the earlier one (Mathis & Whiffen 1989) and with $\rho_0 \simeq 2.8\,\mathrm{g\,cm^{-3}}$; the size distribution of the aggregates peaks at $r \approx 0.16\mu$m; the lower limit of the individual particle size is $a \sim 2$nm. Thus if we substitute the previous values for $\omega, \beta, \bar{E}, \alpha$ and h we obtain $\frac{S}{T_{ag}} > 100$ for $r \geq 0.16\mu$m ! So that even for these rather compact aggregates the larger particles in the size distribution will be blown apart.

8. Albedo

The wavelength dependent albedo (the ratio of the scattering cross section to the extinction), reflecting the scattering properties of the dust particles, provides another constraint on interstellar dust models. In Fig. 12 we plot the theoretical albedos resulting from the finite cylinder particles alone and those from the total model. Note that the hump particles and the PAH's are assumed to be pure absorbing and the scattering part is only contributed by the core-mantle particles although *some* scattering has been attributed in the hump region along the line sight of HD 38087 (Witt et al. 1986). But this probably does not apply to the *general* ISM because the total to selective extinction ratio R_v of HD 38087 is as high as 5.3 (CCM) which indicates the dust grains of HD 38087 are larger than those of the diffuse medium. Also plotted in Fig. 12 are the observational albedos derived from the measurements of the diffuse Galactic light (Lillie & Witt 1976; Morgan 1980) and of a high latitude cloud Lynds 1642 (Laureijs et al. 1987). It can be seen in Fig. 12 that our predicted albedos are in reasonably good agreement with the observations, although the model results are lower than the measurements of Lillie & Witt (1976). Keep in mind that the lack of knowledge of the geometry (Chlewicki & Greenberg 1984), possible contamination by fluorescent emission (Witt 1988), and the fact that the albedo and the asymmetry factor are coupled with each other in the interpretation (i.e., neither the albedo nor the asymmetry factor can be determined independently), could lead to uncertainties in the observed albedos.

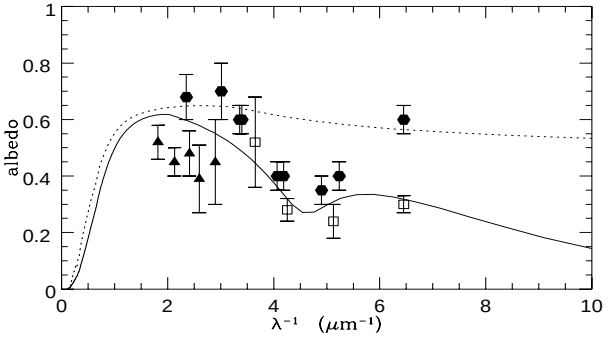

Fig. 12. Comparison of the theoretical albedos predicted by the finite cylinder dust model with observations. Solid line corresponds to the albedo produced by all the dust components together; dotted line corresponds to the albedos produced by large particles alone. The observational data are plotted as: hexagons (Lillie & Witt 1976); triangles (Laureijs et al. 1988); and squares (Morgan 1980).

It is worth noting that our predicted NIR albedos are quite low (~ 0.2 at $\lambda \simeq 2\mu$m), much lower than the measurements of Block et al. (1994) (~ 0.8) and of Lehtinen & Mattila (1996) (~ 0.8). For the former, possible hidden near infrared sources which would raise the albedo of the dust might be suggested in the form of a contribution by a number of cool low mass stars. This remains a conjecture which should be further investigated. Witt et al. (1994) attributed the high albedo to large grain size and to possible contamination of NIR non-equilibrium continuum emission of very small particles which are undergoing temperature fluctuations. For the latter, there is a quite natural explanation because the albedos derived by Lehtinen & Mattila (1996) are for a *dense molecular cloud* ($R_v \simeq 5.3$) where the core-mantle particles are undoubtedly coated with outer ice mantles. The ice mantles are more transparent and contribute more to the scattering than the silicate core-organic refractory mantle. Similarly, the high albedos (~ 0.75 at $\lambda \simeq 2.2\,\mu$m) obtained for an IR reflection nebula by Pendleton et al. (1990) were also accompanied by the presence of ice mantles. Furthermore, the fact that the dust emission at $\lambda \sim 12\mu$m is too weak compared to those at $\lambda \sim 60\mu$m and $\sim 100\mu$m to be detected by IRAS also indicates that the dust particles studied in Lehtinen & Mattila (1996) are dense molecular cloud grains instead of diffuse cloud grains, because, as shown in Greenberg & Li (1996b), the partial depletion of the PAH's (accreted into the ice coated core-mantle particles) in dense molecular clouds would lead to decreased emission in the near/mid infrared ($\lambda \sim 10\,\mu$m) relative to that in the far infrared ($\lambda \sim 60\,\mu$m) because of reduced fluctuating temperature emission (Greenberg 1968). This

also leads to a higher *ultraviolet* albedo because the absorbing hump and PAH particles are depleted while the increase in size of the large particles does not decrease their albedo which is already asymptotic to $\sim 1/2$ in the UV.

9. Cosmic abundance constraint

The three basic considerations underlying the cosmic abundance constraint are: a) that there is a correlation between the amount of dust and the elemental hydrogen; b) that there exists a general average abundance of the "abundant" condensable atom (O, C, N, Mg, Si, Fe) with respect to hydrogen; c) a successful dust model should be consistent with the cosmic abundance constraint, in the sense that the amount of any species x locked up in the dust phase by a model can not exceed the cosmically available amount. Item c may be expressed as follows,

$$\left[\frac{X}{H}\right]_d^{mod} \leq \left[\frac{X}{H}\right]_d^{ava} = \left[\frac{X}{H}\right]_c^{ism} - \left[\frac{X}{H}\right]_g^{ism} \tag{17}$$

where $\left[\frac{X}{H}\right]_c^{ism}$ is the cosmic abundance of the species x relative to hydrogen in the interstellar medium; $\left[\frac{X}{H}\right]_g^{ism}$ is the observed gas phase abundance of the species x; $\left[\frac{X}{H}\right]_d^{ava}$ and $\left[\frac{X}{H}\right]_d^{mod}$ refer to the *available* abundance to be bound in dust grains and the abundance *required* to be bound in dust grains by a dust model, respectively. The major species incorporated into our dust model are C, O, N, Si, Fe, Mg etc. We confine ourselves to considering these elements.

9.1. Dust-gas correlation

It is normally assumed that the dust particles are suspended in and essentially trapped in the gas clouds. Physically, one can anticipate the situation in which various components of the dust may diffuse locally with respect to each other or with respect to the gas because of the phenomena induced by turbulent eddies or differential radiation pressure effects. But, observationally there appears to be a reasonably uniform correlation in the diffuse interstellar medium between the column density of elemental hydrogen (in all forms) and the dust extinction color excess E_{B-V} expressed as $N_H/E_{B-V} = C \times 10^{21}$ cm^{-2} where C is usually taken as $C \equiv 5.9$ (Bohlin et al. 1978). A further assumption is that from this one can deduce a line of sight average volume density of solid material relative to hydrogen. Underlying *this* assumption is the requirement that there is a constant ratio of the *number* of dust particles relative to the number of hydrogen atoms as well as a uniformity of dust properties. If these apply, the correlation may be expressed as $\bar{n}_d/\bar{n}_H = constant$ where $\bar{n}_d$ and $\bar{n}_H$ are the average of the number density of dust particles and of hydrogen. We may now express the correlation factor as

$$\frac{N_H}{E_{B-V}} \Longrightarrow \frac{N_H}{A_v} \Longrightarrow \frac{\bar{n}_H L}{\bar{n}_d \bar{A}_d \bar{Q}_{ext} L} \tag{18}$$

where L is the line-of-sight distance, $\bar{A}_d$ is the mean area of the dust particles contributing to the visual extinction, $\bar{Q}_{ext}$ is the mean extinction efficiency, and where we have assumed a uniformity of dust properties expressed by $A_v/E_{B-V} = constant$. The *total* extinction then implies a mean *area* of dust particles per unit area along the line of sight. The mean particle size is determined by the wavelength dependence of extinction. One may then derive a mean dust volume density along the line of sight, given the $\bar{Q}_{ext}$ which depends on the optical properties of the dust material. Thus, with the assumption of perfect coupling of dust numbers to gas numbers the dust-gas correlation may be reduced to a correlation between *hydrogen* density and *dust volume* density. When the dust properties vary as in molecular clouds or as in the Galactic halo the ratio of dust volume to hydrogen number deduced from N_H/E_{B-V} must be appropriately modified since both the physical coupling of gas to dust and particle size as well as material properties of the dust are different from those in the general diffuse interstellar medium.

9.2. Cosmic abundance

The current ideas about the abundances of the condensable elements in the interstellar medium have undergone a substantial revision from when they were believed to be those of the solar system. At one time it had been thought that the present abundances were established before the solar system was born and have remained relatively constant ever since. While it has long been recognized that abundances are not generally the same spatially such that, for example, the inner regions of galaxies like our own seem to have a greater abundance of heavy elements than the outer region, it was nevertheless assumed that over the regions where the diffuse medium interstellar dust is well understood; i.e., within a few Kpc of the Sun, the mixing maintained a reasonable uniformity. In any case, a direct measure of the elemental abundances in the interstellar medium is impossible unless all the elements are observable as atoms or ions. Even given that no atoms are depleted in the dust, the measurements of the gas phase abundances of some elements are very difficult. The following is based in part on the unpublished notes entitled *"Low CNO Abundances in the ISM?"* compiled with J.A. de Freitas Pacheco during a visiting professorship by one of us (JMG) at the University of Sao Paulo in 1992.

There are data on stars and nebulae which seem to support a paucity of oxygen in the interstellar medium (ISM) relative to the solar system, solving the old controversy about the distinct abundances between the Sun and the ionized gas in Orion.

The evidences for a present lower oxygen abundance are:
1) The analysis of the oxygen abundance in intermediate mass F-K supergiants having main sequence B stars as progenitors, indicates an average value of 8.70 in the logarithmical scale ($12 + log\left[\frac{O}{H}\right]_g^{ism}$) (Luck & Lambert 1985);
2) B stars in associations and young clusters studied by Fitzsimmons et al. (1990) gave an average oxygen abundance of 8.75, suggesting a deficiency of about 0.17 dex with respect to the Sun;
3) Unevolved B stars analyzed by Gies & Lambert (1992) gave similar results. They found an average value of 8.68, pointing

to a similar oxygen underabundance;
4) Cunha & Lambert (1992) have studied the oxygen abundance in evolved B stars in the Orion nebula, concluding that their average value 8.64 is compatible with that of the associated HII region;
5) The average oxygen abundance in HII regions after the extensive work by Shaver et al. (1983) is 8.76, compatible with the results derived from young stars;
6) Abundances in planetary nebulae are less sensitive to model parameters than those derived from star's photospheres. The analysis of type I planetaries, originating from progenitors with masses higher than 2.5 $M_{\odot}$, belonging to the young disk population, have an average oxygen abundance 8.72 (de Freitas Pacheco 1993) entirely compatible with the above results.

The O/Fe behavior with metallicity can be explained in terms of the relative contribution variation of both types of supernovae (Ia & II) to the chemical enrichment of the galactic disk (de Freitas Pacheco 1993).

The situation concerning the carbon and nitrogen abundances in young objects (stars and nebulae) is more uncertain. It would be of interest to note that the solar system C/O ratio found earlier (Cameron 1982; Anders & Ebihara 1982; Grevesse 1984) all gave close to C/O = 0.6 while the latest determined by Grevesse et al. (1996) is 0.48. The results by Gies & Lambert (1992) on unevolved B stars point to an average value of C/O = 0.32. This means that carbon would be *more* deficient than oxygen and underabundant by 0.4 dex with respect to the solar value. However carbon abundance determinations in the Orion nebula suggest a higher ratio, although the results are quite conflicting. Dufour, Shields & Talent (1982) derived C/O = 0.72, a value considerably higher than solar. A still higher value was obtained by Peimbert (1987), C/O = 0.83. A more recent study by Rubin et al. (1991) confirms essentially the result by Peimbert (1987), since those authors obtained C/O = 0.85 from their data. Nevertheless a value closer to solar was obtained by Baldwin et al. (1991), namely, C/O = 0.56. These results suggest that carbon abundance determinations in the nebula are still quite uncertain.

A similar picture is found when the nitrogen data is analyzed. The B stars data by Gies & Lambert (1992) give an N/O ratio similar to the Sun. They have obtained for their sample an average ratio N/O = 0.13 while the solar value is N/O = 0.12. In the Orion nebula (and in other HII regions) the nitrogen abundances determined from the forbidden lines in the visible and in the red of NII are systematically lower than the abundances derived from the FIR lines of NIII (see, for instance, Rubin et al. 1991). The N/O ratio derived from different studies of the Orion nebula has a large spread, varying from 0.076 (Dufour, Shields & Talent 1982) to 0.23 (Baldwin et al. 1991). If, for the same reasons as before, we consider that the star value is actually representative of the ISM, then nitrogen is also presently deficient by the same amount as oxygen.

Averaging the oxygen abundances in young objects (see items 1–6 above) either logarithmically or linearly gives about the same abundance value of $\left[\frac{O}{H}\right]_c^{ism} \approx 512 \times 10^{-6}$. This is about 70% of the solar value of $\left[\frac{O}{H}\right]_c^{\odot} \approx 740 \times 10^{-6}$ (Grevesse et al. 1996). If a solar system ratio of C/O = 0.6 or 0.48 were to apply, this would imply $\left[\frac{C}{H}\right]_c^{ism} \approx 307$ or 250 $\times 10^{-6}$. As we shall see later the latter value seems to present an impossible challenge to *any* dust model. *Is there a problem with the C/O ratio?*

9.3. Cosmic abundance constraint

We first derive the elemental depletion needed for the dust; i.e., $\left[\frac{X}{H}\right]_d^{mod}$. We assume the mass density of the silicate cores to be 3.5 g cm^{-3} and use a chemical composition of that of amorphous olivine, $MgFeSiO_4$. The mass density of the organic refractory mantle is not well determined, but we shall assume it to be 1.8 g cm^{-3} (somewhat lower than amorphous carbon). Both of these densities are possibly too high so that our model elemental requirements may be overestimated perhaps by as much as 20% (for example, the density of terrestrial silicates could be as low as 2.5 g cm^{-3}). The relative atomic composition of the mantle is assumed to be $C : O : N : H$ = 1.0 : 0.2 : 0.04 : 1.0 which is based on the measurements of laboratory organics and the Comet Halley mass spectra (Greenberg et al. 1993; Schutte 1988; Krueger & Kissel 1987). We adopt 2.3 g cm^{-3} and 2.4 $\times$ 10^{-7} g cm^{-2} as the mass density of the hump particles and the PAH's (assumed to be essentially 2 dimensional) respectively. From the number densities n_{cm}, n_{hump}, n_{PAH} and the sizes determined in Sect. 5.2 and 6 for fitting the interstellar extinction curve and the polarization law (see Table 1), and the above assumed mass densities as well as the chemical compositions, we can obtain $\left[\frac{X}{H}\right]_d^{mod}$, the amount of each species x locked in the dust particles. The results are given in Table 2.

The observed gas phase abundances were summarized in van Dishoeck et al. (1993). Recently, high signal-to-noise observations with the Goddard High Resolution Spectrograph (GHRS) aboard the Hubble Space Telescope showed that $\left[\frac{C}{H}\right]_g^{ism} \approx 140 \pm 20 \times 10^{-6}$ (Cardelli et al. 1996), $\left[\frac{O}{H}\right]_g^{ism} \approx 310 \pm 20 \times 10^{-6}$ (Meyer et al. 1994) both of which show no variation in different lines of sight and different physical conditions. This invariance seems strange to us because it implies no variation in dust properties in terms of depletion. In fact this is the kind of phenomenon which led one of us (JMG) 20 years ago to question the depletion then "derived". The GHRS observations of MgII, SiII, FeII etc. made by Sembach & Savage (1996) toward the *diffuse halo clouds* gave $\left[\frac{Mg}{H}\right]_g^{ism} \approx 11.7 \times 10^{-6}$, $\left[\frac{Fe}{H}\right]_g^{ism} \approx 7.41 \times 10^{-6}$, $\left[\frac{Si}{H}\right]_g^{ism} \approx 19.5 \times 10^{-6}$. The average interstellar gas phase abundances of Mg, Fe, and Si should be much lower than these quantities because, as shown in Sembach & Savage (1996), the gas phase abundances increase progressively from the Galactic disk to halo. This could be caused by a combination of the following facts: 1) supernova explosions may sweep gas and dust into the halo as a "Galactic fountain"; 2) the radiation pressure from the Galactic plane stars may also

Table 2. Heavy element depletions in the diffuse cloud determined from the finite cylinder model ($\rho_{si} \simeq 3.5$ g cm^{-3}, $\rho_{or} \simeq 1.8$ g cm^{-3}).

element	core-mantle		hump	PAH	total
	core	mantle			
Si	2.04×10^{-5}	-	-	-	2.04×10^{-5}
Fe	2.04×10^{-5}	-	-	-	2.04×10^{-5}
Mg	2.04×10^{-5}	-	-	-	2.04×10^{-5}
C	-	1.08×10^{-4}	3.74×10^{-5}	4.87×10^{-5}	1.94×10^{-4}
O	8.16×10^{-5}	2.16×10^{-5}	-	-	1.03×10^{-4}
N	-	4.3×10^{-6}	-	-	4.3×10^{-6}

expel gas and dust into the halo (Greenberg et al. 1987b); and 3) the dust grains in the halo clouds suffer more severe and more frequent shocks than in the disk. All of these result in higher halo gas phase abundances of the refractory elements. We believe that, generally, Mg, Fe, and Si are highly depleted so that their dust phase abundances are close to their cosmic abundances. Therefore, for Mg, Fe, and Si, we will compare $\left[\frac{X}{H}\right]_d^{mod}$ with $\left[\frac{X}{H}\right]_c^{ism}$ rather than with $\left[\frac{X}{H}\right]_d^{ava}$; i.e., we assume $\left[\frac{X}{H}\right]_g^{ism} / \left[\frac{X}{H}\right]_c^{ism} \ll 1$.

Are the elemental depletions in our model consistent with the cosmic abundance constraint? The answer to this depends on the "reference abundance"; i.e., $\left[\frac{X}{H}\right]_c^{ism}$, the cosmic abundance. Historically, the interstellar medium was assumed to have the same composition as the solar system; i.e., the solar cosmic abundances $\left[\frac{X}{H}\right]_c^{\odot}$ were adopted as the "reference abundance" $\left[\frac{X}{H}\right]_c^{ism}$. Table 3 lists the solar system abundances $\left[\frac{X}{H}\right]_c^{\odot}$ (Grevesse et al. 1996) and the amount of the remaining atoms which could be locked in dust grains, $\left[\frac{X}{H}\right]_d^{ava\odot}$, obtained by subtracting the gas phase abundances $\left[\frac{X}{H}\right]_g^{ism}$. Obviously, our model required abundances $\left[\frac{X}{H}\right]_d^{mod}$ are within the solar system "cosmic" abundances constraint. As a matter of fact, *all* the existing dust models are consistent with the cosmic abundances if the solar system abundances are adopted as the "reference abundance".

However, as seen in Table 3, almost all $\left[\frac{X}{H}\right]_d^{mod}$ are appreciably less than $\left[\frac{X}{H}\right]_d^{ava\odot}$ which indicates that, in the interstellar space, there are many *more* atoms than could be accounted for in the dust and gas. This was pointed out over 20 years ago by Greenberg (1974) as a problem *"Where have all those atoms gone ?"* A promising solution, extensively discussed recently, is that the actual interstellar abundances are appreciably less than the solar abundances, probably $\left[\frac{X}{H}\right]_c^{ism}$ may be only 60%–70% of $\left[\frac{X}{H}\right]_c^{\odot}$ (Greenberg & de Freitas Pacheco 1992; Cardelli et al. 1996; Snow & Witt 1996; Mathis 1996; Sect. 9.2). It has been suggested that the solar abundances could have been enhanced by the injection of nucleosynthetic products of a nearby supernova into the solar system (Olive & Schramm 1982) and may not be representative of the cosmic abundances. Another possibility is that the explosion rate of type II supernovae has been decreasing with a resulting secular decrease in the heavier elements in the past 5 billion years. If it really is the case that the solar system abundances are too high, the new "reference abundance" will provide a serious challenge to the dust models.

We list in Table 3 $\left[\frac{X}{H}\right]_c^{\frac{2}{3}\odot}$ and $\left[\frac{X}{H}\right]_d^{ava\frac{2}{3}\odot}$ if we adopt $2/3$ of the solar abundances as the interstellar abundances. Also shown are $\left[\frac{X}{H}\right]_d^{mod}$ required by other models (MRN; Hong & Greenberg 1980; Draine & Lee 1984; Mathis & Whiffen 1989; Kim, Martin & Hendry 1994). The abundances for the latest composite dust model (Mathis 1996) are not included in the table because the required carbon abundances vary in a wide range, depending on the adopted carbon materials: amorphous carbon (AMC), graphite, organic refractory, HAC, etc.

Table 3 shows that, with the assumption that the interstellar abundances are $2/3$ the Grevesse et al. (1996) solar system abundances, *all* the dust models consume *more* than the *available* carbon atoms. Moreover, all the dust models, except our current work, have a crisis not only for carbon but also for all the other species. Although amongst the existing models, ours uses the least carbon, we are not totally relieved either. It must be admitted here that this was what gave rise to the question by one of us (JMG) of whether the severity of the reduced carbon abundance as initially considered by Greenberg & de Freitas Pacheco (1992) was real. Now the question is not *"Where have all those atoms gone ?"* but *"Where can we find them ?"*. Among the possible answers are: 1) that we have overestimated the dust requirement by overestimating the constituent densities of the core and mantle materials; 2) that the "reference abundance" is underestimated by using $2/3$ of the Grevesse et al. (1996) solar system value. If the current C/O ratio is 0.6, then the cosmic abundance of carbon is raised to $\left[\frac{C}{H}\right]_c^{\frac{2}{3}\odot} \approx 296 \times 10^{-6}$ so the available carbon $\left[\frac{C}{H}\right]_d^{ava\frac{2}{3}\odot} \approx 156 \times 10^{-6}$. If we assume $\rho_{si} \simeq 2.8$ g cm^{-3}, $\rho_{or} \simeq 1.44$ g cm^{-3}; i.e., $\sim 20\%$ lower than adopted in Table 2, the required dust carbon is lowered to $\left[\frac{C}{H}\right]_d^{mod} \approx 172 \times 10^{-6}$. This is certainly coming within the observational errors. Also if we adopt $\left[\frac{C}{H}\right]_c^{\odot} \approx 487 \times 10^{-6}$ (Meyer 1988) rather than $\left[\frac{C}{H}\right]_c^{\odot} \approx 355 \times 10^{-6}$ (Grevesse et al. 1996), then $\left[\frac{C}{H}\right]_d^{ava\frac{2}{3}\odot} \approx 185 \times 10^{-6}$ which is already acceptable even without questioning the dust material densities.

Table 3. The cosmic abundance constraint (in unit of atoms per 10^6 hydrogen nuclei).

element	gas phase	solar†		2/3 solar‡		$\left[\frac{X}{H}\right]_d^{mod}$ for dust models⋆					
X	$\left[\frac{X}{H}\right]_g^{ism}$	$\left[\frac{X}{H}\right]_c^{\odot}$	$\left[\frac{X}{H}\right]_d^{ava\odot}$	$\left[\frac{X}{H}\right]_c^{\frac{2}{3}\odot}$	$\left[\frac{X}{H}\right]_d^{ava\frac{2}{3}\odot}$	This work	MRN	DL	KMH	MW	HG
Si	$\oplus$	36.0 ± 4	36.0 ± 4	24.0	24	20.4	31	32	33.7	-	30
Fe	$\oplus$	31.6 ± 3	31.6 ± 3	21.1	21	20.4	26	29	-	-	26
Mg	$\oplus$	38.0 ± 4	38.0 ± 4	25.3	25	20.4	33	35	-	-	33
C	140 ± 20	355 ± 40	215	237	97^a	194^b	≥ 240	300	300	300	280
O	310 ± 20	740 ± 120	430	493	183	103	-	128	-	-	444
N	61	93 ± 14	32	62 ± 9	1.0 ± 9	4.3	-	-	-	-	57

† The "reference abundance" is assumed to be the solar system abundance (Grevesse et al. 1996).
‡ The "reference abundance" is assumed to be $2/3$ of the solar system abundance (Grevesse et al. 1996).
⋆ MRN = Mathis, Rumpl & Nordsieck (1977); DL = Draine & Lee (1984); KHM = Kim, Martin & Hendry (1994); MW = Mathis & Whiffen (1989); HG = Hong & Greenberg (1980). − means that no explicit number was given.
$\oplus$ Assuming very low gas phase abundance for Si, Fe, Mg.
[a] This could be ~ 160 as discussed in text.
[b] This could be ~ 170 as discussed in text.

A final note is that, the gas phase carbon abundance in IC 63, a reflection nebula, is only $\simeq 50 \times 10^{-6}$ (Jansen et al. 1995), which is much less than the value ($\simeq 140 \times 10^{-6}$) obtained by Cardelli et al. (1996). After all, it is already noted by Grevesse et al. (1996) that ".... the uncertainties are still uncomfortably large ....". Other factors which could reduce the dust requirement are that the optical constants of the dust particles may actually be a bit higher. Finally, returning to one of the basic dust/gas assumptions, there are still some uncertainties in the A_v/N_H ratio. Overall, in our estimation it is not difficult to see why the unified dust model as proposed is already close enough in the required atomic composition to avoid the so-called "carbon crisis" by at least a factor of $2/3$ (coincidental factor) relative to all other dust models. In fact, we are quite satisfied to have answered the original question about *"Where have all those atoms gone ?"* without introducing a new one.

10. Summary

The latest spectroscopic observational data and laboratory measurements on organic refractories and silicates have been used to obtain the wavelength dependence of the optical constants of the core and the mantle components of interstellar dust grains. The derived size distribution of silicate core-organic refractory mantle particles with an elongation of two which leads to a fit to the average diffuse cloud interstellar polarization from the near infrared to the far ultraviolet provides the major contribution to the infrared and visual extinction. The model, with no further adjustment of parameters, automatically gives the observed so-called "excess" continuum polarization between 2 μm and 5 μm as well as the 10 μm and 20 μm polarization towards the Becklin-Neugebauer object.

The unification of the source of the full polarization and the major infrared to near ultraviolet extinction by the core-mantle particles alone makes it possible to obtain a polarization to extinction ratio in the visual which is comfortably larger than the maximum observed value of $(P/A)_v = 0.03$. It is confirmed that the polarization to extinction ratio by infinite cylindrical particles is twice that of the finite $(2:1)$ particles at all wavelengths observed. The polarization to extinction maximum given by the silicate/graphite interstellar dust model fails to satisfy the condition imposed by the maximum observed value. Composite dust models of low density which satisfy the $(P/A)_v$ constraint are required to spin at angular velocities which cause the large particles to break up by centrifugal forces greater than their tensile strength.

The evidence for a reduced abundance of the condensable elements (C, O, N, Si, Mg, Fe) relative to the solar system abundance is extensively discussed. This leads to rather stringent constraints on dust models of which we were not aware when, on the contrary, the solar system abundance led to an overabundance expressed by "*The interstellar depletion mystery or where have all those atoms gone ?"*. The new model satisfies all currently accepted abundance limitations for O, N, Mg, Fe, Si but leaves a possible problem for C. It is certainly closer to satisfying this constraint than any other reasonable dust models and the slight extra amount required appears to be well within the uncertainties of the interstellar constraint.

Because the optical constants all satisfy the Kramers-Kronig relation the wavelength dependence of the circular polarization satisfies the observational condition of passing through zero at the wavelength of maximum linear polarization.

Finally, the albedo calculated for the full complement of dust components is consistent with observations.

Acknowledgements. We are grateful for the support by NASA grant NGR 33-018-148 and by a grant from the Netherlands Organization for Space Research (SRON). We thank the Dutch Stichting Nationale Computer Faciliteiten (NCF) for providing the Cray Y-MP supercomputer time. We thank Dr. Willem Schutte for helpful discussions on the organic refractory composition. One of us (JMG) wishes to thank the University of Sao Paulo (Institute of Astronomy and Geophysics)

for a visiting professorship in 1992 which provided an opportunity to work with Dr. P.D. Singh, Dr. A.A. de Almeida and Dr. J.A. de Freitas Pacheco. One of us (AL) wishes to thank the World Laboratory for a fellowship. AL is also grateful to Dr. Francois Rouleau for his help in using the supercomputer.

References

Aannestad, P.A. & Kenyon, S.J. 1979, ApJ 230, 771
Allamandola, L.J., Tielens, A.G.G.M & Barker, J.R. 1989, ApJS 71, 733
Anders, E. & Ebihara, M. 1982, Geochim. Cosmochim. Acta 46, 2363
Anderson, C.M. et al. 1996, AJ 112, 2726
Asano, S. & Yamamoto, G. 1975, Appl. Opt. 14, 29
Baldwin, J.A., Ferland, G.J., Martin, P.G., Corbin, M.R., Cota, S.A., Peterson, B.M. & Slettebak, A. 1991, ApJ 374, 580
Barber, P.W. & Yeh, C. 1975, Appl. Opt. 14, 2864
Barber, P.W. & Hill, S.C. 1990, Light Scattering by Particles: Computational Methods, World Scientific, Singapore
Blanco, A., Fonti, S. & Orofino, V. 1996, ApJ 462, 1020
Block, D.L., Witt, A.N., Grosbol, P., Stockton, A. & Moneti, A. 1994, A&A 288, 383
Bohren, C.F. & Huffman, D.R., 1983, Absorption and Scattering of Light by Small Particles, Wiley, New York
Bohlin, R.C., Savage, B.D. & Drake, J.F. 1978, ApJ 224, 132
Bussoletti, E., Colangeli, L., Borghesi, A. & Orofino, V. 1987, A&AS 70, 257
Cameron, A.G.W. 1982, in: Essays in Nuclear Astrophysics, C.A. Bornes & D.D. Clayton & D.N. Schramm (eds), Cambridge University Press, p.23
Cardelli, J.A., Clayton, G.C. & Mathis, J.S. 1989, ApJ, 245, 345
Cardelli, J.A., Meyer, D.N., Jura, M. & Savage, B.D. 1996, ApJ, 467, 334
Chlewicki, G. & Greenberg, J.M., 1984, MNRAS 210, 791
Chlewicki, G., 1985, Observational Constraints on Multimodal Interstellar Grain Populations, PhD Thesis, Leiden University
Chlewicki, G. & Greenberg, J.M., 1990, ApJ 365, 230
Clayton, G.C. et al. 1992, ApJ 385, L53
Clayton, G.C., Wolff, M.J., Allen, R.G. & Lupie, O. 1995, ApJ 445, 947
Cohen, M., Tielens, A.G.G.M. & Bregman, J.D., 1989, ApJ 344, L13
Coyne, G.V., Gehrels, T. & Serkowski, K. 1974, AJ 79, 581
Cronin, J.R. & and Pizzarello, S. 1990, Geochim. Cosmochim. Acta 54, 2859
Cunha, K. & Lambert, D.L. 1992, ApJ 399, 586
David, P. & Pégourié, B., 1995, A&A 293, 833
de Groot, M., van der Zwet, G.P., Jenniskens, P., Bauer, R., Baas, F. & Greenberg, J.M., 1988, in: Dust in the Universe, Bailey, M.E. & Williams, D.A. (eds), Cambridge Press, p.265
Désert, F.X., Boulanger, F. & Puget, J.L., 1990, A&A 237, 215
Dorschner, J., Begemann, B., Henning, Th., Jäger, C. & Mutschke, H., 1995, A&A 300, 503
Dorschner, J. & Henning, Th. 1995, A&A Rev. 6, 271
Draine, B.T. & Salpeter, E.E. 1979a, ApJ 231, 77
Draine, B.T. & Salpeter, E.E. 1979b, ApJ 231, 438
Draine, B.T. & Lee, H.M. 1984, ApJ 285, 89
Draine, B.T. 1988, ApJ 333, 848
Draine, B.T. & Malhotra, S. 1993, ApJ 414, 632
Dufour, R.J., Shields, G.A. & Talent, R.J.Jr 1982, ApJ 252, 461
Duley, W.W., Jones, A.P. & Williams, D.A. 1989, MNRAS 236, 709
Ehrenfreund, P., Robert, F., d'Hendecourt, L. & Behar, F. 1991, A&A 252, 712
Fitzpatrick, E.L. & Massa, D. 1986, ApJ 307, 286
Fitzsimmons, A., Brown, P.J.F., Dufton, P.L. & Lennon, D.J. 1990, A&A 232, 437
de Freitas Pacheco, J.A. 1993, ApJ 403, 673
Gilra, D.P. 1972, in: The Scientific Results from the Orbiting Astronomical Observatory OAO-2, Code, A.D. (ed.), NASA SP-310, 295
Gies, D.R. & Lambert, D.L. 1992, ApJ 387, 673
Greenberg, J.M. & Shah, G.A. 1966, ApJ 145, 63
Greenberg, J.M., 1968, in: Stars and Stellar Systems, Vol. VII, Middlehurst, B.M. & Aller, L.H. (eds.), University of Chicago Press, p.221
Greenberg, J.M., Yencha, A.J., Corbett,J.W. & Frisch, H.L. 1972, Mem. Soc. Roy. des Sciences de Liege, 6e Serie, tome IV, p.425
Greenberg, J.M. 1974, ApJ 189, L81
Greenberg, J.M. & Hong, S.S., 1974a, in: IAU Symposium 60, Galactic and Radio Astronomy, Kerr, F. & Simonson, S.C. (eds), Dordrecht : Reidel, p.155
Greenberg, J.M. & Hong, S.S., 1974b, in: HII regions and the Galactic center, Moorwood, A.F.M. (ed), ESRSOSP-105, p.153
Greenberg, J.M., 1982, in: Submillimetre Wave Astronomy, Beckman, J.E. & Phillips, J.P.(eds), Cambridge University Press, p.261
Greenberg, J.M. & Chlewicki, G. 1983, ApJ 272, 563
Greenberg, J.M., 1986, in: Light on Dark Matter, Israel, F.(ed.), Reidel, Dordrecht, p.177
Greenberg, J.M., de Groot, M.S. & van der Zwet, G.P. 1987a, in: Polycyclic Aromatic Hydrocarbons and Astrophysics, A. Léger, L. d'Hendecourt & N. Boccara (eds), Kluwer, p.177
Greenberg, J.M., Ferrini, F., Barsella, B. & Aiello, S. 1987b, Nature 327, 6119
Greenberg, J.M. & de Freitas Pacheco, J.A. 1992, unpublished
Greenberg, J.M., Mendoza-Gómez, C.X., de Groot, M.S. & Breukers, R. 1993, in: Dust and Chemistry in Astronomy, T.J. Millar & D.A. Williams (eds.), IOP publ. Ltd., p.265
Greenberg, J.M., Mizutani, H. & Yamamoto, T. 1995, A&A 295, L35
Greenberg, J.M. & Li, A., 1995, in: The Opacity of Spiral Disks, J.I. Davies & D. Burstein (eds), Dordrecht, Kluwer, p.19
Greenberg, J.M., Li, A., Mendoza-Gómez, C.X., Schutte, W.A., Gerakines, P.A. & de Groot, M. 1995, ApJ 455, L177
Greenberg, J.M. & Li, A. 1996a, A&A 309, 258
Greenberg, J.M. & Li, A. 1996b, in: New Extragalactic Perspectives in the New South Africa, Block, D.L. & Greenberg, J.M. (eds), Kluwer, p.118
Greenberg, J.M. & Li, A. 1996c, in: The Cosmic Dust Connection, J.M. Greenberg (ed.), Kluwer, Dordrecht, p.43
Grevesse, N. 1984, Physica Scripta 78, 49
Grevesse, N., Noels, A. & Saural, A.J. 1996, in: Cosmic Abundances, S.S. Holt & G. Sonneborn (eds), ASP Conf. Series, Vol. 99, p.117
Hage, J.I. & Greenberg, J.M. 1990, ApJ 361, 251
Holt, A.R., Uzunoglu, N.K. & Evans, B.G. 1978, IEEE Trans., Ap-26, 706
Hong, S.S. & Greenberg, J.M. 1980, A&A 88, 194
Huffman, D. & Stapp, J.L. 1973, in: IAU Symp. 52, Interstellar Dust and Related Topics, J.M. Greenberg & H.C. van de Hulst (eds), Reidel, p.297
Jansen, D.J., van Dishoeck, E.F., Keene, J.B., Boreiko, R. & Betz, A.L., 1996, A&A 309, 899
Jenniskens, P. 1993, A&A 274, 653
Jenniskens, P., Baratta, G.A., Kouchi, A., de Groot, M.S., Greenberg, J.M. & Strazzulla, G., 1993, A&A 273, 583

Joblin, C., Léger, A. & Martin, P. 1992, ApJ 393, L79
Jones, A.P., Tielens, A.G.G.M., Hollenbach, D.J. & McKee, C.F. 1994, ApJ 433, 797
Jones, T.W. & Merrill, T.M. 1977, ApJ 209, 509
Jura, M. 1986, ApJ 303, 327
Kim, S.H., Martin, P.G. & Hendry, P.D. 1994, ApJ 422, 164
Kim, S.H. & Martin, P.G. 1994, ApJ 431, 783
Kim, S.H. & Martin, P.G. 1995a, ApJ 444, 293
Kim, S.H. & Martin, P.G. 1995b, ApJ 442, 172
Krueger, F.R. & Kissel, J. 1987, Naturwissenschaften 44, 312
Kuik, F., de Haan, J.F. & Hovenier, J.W. 1994, Appl. Opt. 33, 4906
Lamy, P.L. 1978, Icarus 34, 68
Laureijs, R.J., Mattila, K. & Schnur, G. 1987, A&A 184, 269
Lehtinen, K. & Mattila, K. 1996, A&A 309, 570
Léger, A., et al. 1989, in: IAU Symposium 135, Interstellar Dust, L.A. Allamandola & A.G.G.M. Tielens (eds), Kluwer, p.173
Lillie, C.F. & Witt, A.N. 1976, ApJ 208, 64
Lind, A.C. & Greenberg, J.M. 1966, J. of Appl. Phys. 37, 3195
Luck, R.E. & Lambert, D.L. 1985, ApJ 298, 782
Martin, P.G. & Angel, R.P. 1976, ApJ 207, 126
Martin, P.G. 1978, Cosmic Dust, Oxford University Press, Oxford
Martin, P.G. & Whittet, D.C.B. 1990, ApJ 357, 113
Martin, P.G. et al. 1992, ApJ 392, 691
Massa, D., Savage, B.D. & Fitzpatrick, E.L. 1983, ApJ 266, 662
Mathis, J.S., Rumpl, W. & Nordsieck, K.H. 1977, ApJ 217, 425
Mathis, J.S. 1986, ApJ 308, 281
Mathis, J.S. & Whiffen, G. 1989, ApJ 341, 808
Mathis, J.S. 1994, ApJ 422, 176
Mathis, J.S. 1996, ApJ 472, 643
McKee, C.F. 1989, in: IAU Symposium 135, Interstellar Dust, L.A. Allamandola & A.G.G.M. Tielens (eds), Kluwer, p.431
McMillan, R.S. & Tapia, S. 1977, ApJ 212, 714
Meyer, D.M., Jura, M.J., Hawkins, I. & Cardelli, J.A. 1994, ApJ 437, L59
Meyer, J.P. 1988, in: Origin and Distribution of the Elements, G.J. Mathews (ed), World Scientific, Singapore
Mie, G. 1908, Ann. Phys., NY 25, 377
Morgan, D.H. 1980, MNRAS 190, 825
Olive, K.A. & Schramm, D.N. 1982, ApJ 257, 276
Papoular, R., Guillois, O., Nenner, I., Perrin, J.M., Reynaud, C. & Sivan, J.P. 1995, Planet. Space Sci. 63, 1287
Peimbert, M. 1987, in: Star Forming Regions, M. Peimbert & Jugaku, J.(eds), Kluwer, p.111
Pendleton, Y.J., Tielens, A.G.G.M. & Werner, M.W. 1990, ApJ 349, 107
Pendleton, Y.J., Sandford, S.A., Allamandola, L.J., Tielens, A.G.G.M. & Sellgren, K. 1994, ApJ 437, 683
Purcell, E.M. 1979, ApJ 231, 404
Purcell, E.M. & Pennypacker, C.R. 1973, ApJ 186, 705
Roche, R.F. & Aitken, D.K. 1984, MNRAS 208, 481
Rogers, C. & Martin, P.G. 1979, ApJ 228, 450
Rogers, C., Martin, P.G. & Crabtree, D.R. 1983, ApJ 272, 175
Rouleau, F. 1996, A&A 310, 686
Rubin, R.H., Simpson, J.P., Haas, M.R. & Erickson, E.F. 1991, ApJ 374, 564
Sakata, A., Wada, S., Tokunaga, A.T., & Narisawa, T. 1995, Planet. Space Sci. 63, 1223
Sandford, S.A., Allamandola, L.J., Tielens, A.G.G.M., Sellgren, K., Tapia, M. & Pendleton, Y. 1991, ApJ 371, 607
Savage, B.D. & Mathis, J.S., 1979, ARA&A, 17, 73
Schutte, W.A., Tielens, A.G.G.M. & Allamandola, L.J., 1993, ApJ, 415, 397
Schutte, W.A., 1988, The Evolution of Interstellar Organic Grain Mantles, PhD Thesis, Leiden
Scott, A. & Duley, W.W. 1996, ApJS 105, 401
Sembach, K.R. & Savage, B.D. 1996, ApJ 457, 211
Serkowski, K. 1973, in: IAU Symp. 52, Interstellar Dust and Related Topics, J.M. Greenberg & H.C. van de Hulst (eds), Reidel, p.145
Shah, G.A. 1970, MNRAS 148, 93
Shaver, P.A., McGee, R.X., Newton, L.M., Danks, A.C. & Pottasch, S.R. 1983, MNRAS 204, 53
Siebenmorgen, R. & Krügel, E., 1992, A&A, 259, 614
Snow, T.P. & Witt, A.N. 1996, ApJ 468, L65
Somerville, W., et al. 1994, ApJ 427, L47
Sorrel, W.H. 1989, MNRAS 214, 89
Spitzer, L. & Mc Glynn, T.A., 1979, ApJ 231, 417
van de Bult, C.E.P.M., Greenberg, J.M. & Whittet, D.C.B. 1985, MNRAS 214, 289
van de Hulst, H.C., 1957, Light Scattering by Small Particles, Wiley
van Dishoeck, E.F., Blake, G.A., Draine, B.T. & Lunine, J.I., 1993, in: Protostars & Planets III, Levy, E.H. & Lunine, J.I. (eds), University of Arizona Press, p.163
Voshchinnikov, N.V. & Farafonov, V.G. 1993, Ap&SS 204, 19
Waterman, P.C. & McCarthy, C.V. 1968, Mitre Corporation Report MTP-74, Bedford, Massachusetts
Whittet, D.C.B., Martin, P.G., Hough, J.H., Rouse, M.F., Bailey, J.A. & Axon, D.J. 1992, ApJ 386, 562
Wilking, B.A., Lebofsky, M.J. & Rieke, G.H. 1982, AJ 87, 695
Witt, A.N., Bohlin, R.C. & Stecher, T.P. 1986, ApJ 305, L23
Witt, A.N. 1988, in: Dust in the Universe, Bailey, M.E. & Williams, D.A.(eds.), Cambridge Univ. Press, p.1
Witt, A.N., Lindell, R.S., Block, D.L. & Evans, R. 1994, ApJ 427, 227
Wolff, M.J., Clayton, G.C. & Meade, M.R. 1993, ApJ 403, 722
Wright, E.L. 1987, ApJ 320, 818
Xing, Z.F., 1993, Fundamentals of Electromagnetic Theory with Applications to Interstellar Dust, PhD Thesis, Leiden

This article was processed by the author using Springer-Verlag LaTeX A&A style file *L-AA* version 3.